Modeling and Analysis of Circulating Currents Among Input-Parallel Output-Parallel Nonisolated Converters

Yanghong Xia, *Student Member, IEEE*, Miao Yu, *Member, IEEE*, Yonggang Peng, *Member, IEEE*, and Wei Wei

***Abstract*—Input-parallel output-parallel (IPOP) nonisolated converters, including dc/dc and dc/ac converters, are effective solutions to increase the power rating and to improve the reliability of the system. For the safe and steady operation of these IPOP nonisolated converters, the circulating currents are the main challenge, whose detailed mathematic model and corresponding characteristics are not well studied. This paper focuses on the modeling and analysis of circulating currents among these IPOP converters by deriving the detailed mathematic model. Through these models, the complicated characteristics of the circulating currents are presented, which shows that there are various types of circulating currents including circulating currents within the single converter and circulating currents among the multiple converters. It is first demonstrated that the circulating currents will cause port degradation of the converter, that is, the positive and negative currents of the converter are unequal, which makes some port-based control methods ineffective and influences the relay protection. Furthermore, the corresponding influence factors, including line resistances, filters, and so on, are analyzed in detail, especially the asymmetry of line resistances will cause large circulating currents even resulting in instability. It is also found that the traditional control methods cannot completely eliminate these circulating currents because of the strong coupling and complexity of IPOP nonisolated converters. All the theoretical analyses are verified by the real-time hardware-in-loop (HIL) tests.**

***Index Terms*—Circulating currents, input-parallel output-parallel (IPOP) converters, nonisolated converters, port degradation.**

NOMENCLATURE

IPOP	Input-parallel output-parallel.
ISOP	Input-separated output-parallel.
IPOS	Input-parallel output-separated.
BDDC	Bidirectional dc/dc converter.
SDAC	Single-phase dc/ac converter.
TDAC	Three-phase dc/ac converter.
RES	Renewable energy source.
HIL	Hardware in loop.

Manuscript received July 24, 2017; revised October 5, 2017; accepted November 20, 2017. Date of publication December 4, 2017; date of current version July 15, 2018. This work was supported by the National Key R&D Program of China under Grant 2017YFB0902002, the Science and Technology Project of the State Grid Corporation of China under Grant SGBJDK00DWJS1700158, the National Natural Science Foundation of China under Grant 51377142, and the Zhejiang Provincial Natural Science Foundation of China under Grant LY16E070002. Recommended for publication by Associate Editor M. T. Bina. *(Corresponding Author: Miao Yu.)*

The authors are with the College of Electrical Engineering, Zhejiang University, Hangzhou 310027, China (e-mail: royxiayh@126.com; zjuyumiao@zju.edu.cn; pengyg@zju.edu.cn; wwei@zju.edu.cn).

Color versions of one or more of the figures in this paper are available online at http://ieeexplore.ieee.org.

Digital Object Identifier 10.1109/TPEL.2017.2777604

I. INTRODUCTION

THE modern power demands are more and more various, especially more and more dc loads and renewable energy sources (RESs) are integrated into the power system. Therefore, the existing ac distribution network should change to accommodate these dc components. In particular, the hybrid ac/dc distribution network is an effective solution because it can exploit the prominent features of both ac and dc power systems, and thus, the efficiency of the whole system can be enhanced a lot [1]–[4]. The power electronic devices, including bidirectional dc/dc converters (BDDCs), single-phase dc/ac converters (SDACs), and three-phase dc/ac converters (TDACs) are very critical to transfer energy and convert voltage levels in the hybrid ac/dc distribution network. A typical topology of the hybrid ac/dc distribution network is presented in Fig. 1; there are three-phase ac industrial power systems, single-phase ac residential power systems, medium-voltage dc industrial systems, and low-voltage dc residential systems, among which lots of power electronic devices transfer energy and convert voltage levels.

As Fig. 1 shows, the input-parallel output-parallel (IPOP) converters are widely adopted in the system, because there are several advantages of this structure [5]–[7]. First, due to the limitation of power rating of switching devices and the economic consideration, the single converter is hard to transform large power, the IPOP converters can allow the use of low-power converter modules for high-power applications. Second, the IPOP converters can realize higher global efficiency and better thermal distribution, which can simplify the auxiliary design. Third, the IPOP converters have intrinsic redundancy and can provide ride-through capability when one of these converters fails. Hence, the system reliability is improved. However, there are also some challenges for the good operation of IPOP converters, among which the main challenge is the circulating currents. The circulating currents can increase the current stress on the switching devices, degrade system efficiency, or even cause system breakdown if not dealt with appropriately.

See http://www.ieee.org/publications_standards/publications/rights/index.html for more information.

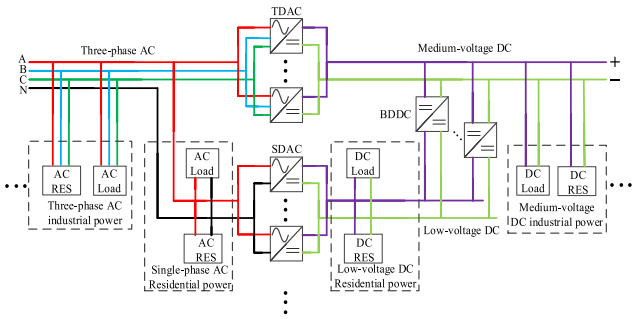

Fig. 1. Typical topology of a hybrid ac/dc distribution network.

In the dc system, the analysis and suppression of circulating currents among IPOP bidirectional dc/dc converters (BDDCs) are widely researched. High-frequency isolation transformers can decouple the input side and output side, which can reduce circulating currents and can simplify the suppression strategies [7]–[11]. By utilizing a common-duty-ratio control scheme, the currents of multiple isolated dual-active half-bridge dc/dc converters can be shared accurately [7]. Analogously, the automatic current sharing are realized among multiple isolated half-bridge dc/dc converters with chain-connected rectifiers based on the common-duty-ratio control scheme [8]. But the common-duty-ration control scheme basically treats the parallel converters as one converter, which makes the extension of converters inconveniently and has less redundancy. Inspired by the IPOP structure, an isolated dc/dc converter with IPOP circuit topology with low-power switching devices is designed in [9] to meet the high-power demand, which can reduce switch count and also the sizes of isolation transformers and passive components. Although this kind of converter need not consider circulating currents, the redundancy and extension are greatly influenced. In [10], IPOP isolated three-level dc/dc converters with an interleaving control strategy are proposed. They can minimize and balance the capacitor ripple currents, hence, the circulating currents can be suppressed. Similarly, the extension is influenced because of the interleaving control strategy. Based on magnetic-coupling current-balancing cells, IPOP LLC resonant converter modules are proposed in [11], which can work well under open-loop operating condition naturally.

The aforementioned methods are based on the high-frequency isolation transformers, which are bulk and expensive. They may also suffer from both core and copper losses, hence, the efficiency and power density of the system are decreased. As a result, some analyses and suppression strategies focusing on IPOP nonisolated dc/dc converters are proposed [12]–[14]. Through some simplifications, the model of circulating currents among IPOP nonisolated dc/dc converters is established in [13] and [14]. Furthermore, treating parallel converters as a whole, interleaved multiphase PWM schemes are proposed to reduce circulating currents. As mentioned earlier, the redundancy and extension are greatly influenced. These approaches are not suitable for modular application. When more converters are connected, the control system becomes very complicated to design. On the other hand, the derived model of circulating currents is not very comprehensive, especially the port degradation (that is the positive and negative currents of one converter are unequal) is not discussed.

In the ac system, the studies about circulating currents among IPOP single-phase dc/ac converters (SDACs) are not very much [15]–[19], while most are focused on circulating currents among IPOP three-phase dc/ac converters (TDACs) [5], [6], [20]–[27]. By analyzing the operation states of IPOP SDACs, the circulating currents along dc loops and ac loops are clearly presented in [15]. And from the point of common mode and differential mode, a centralized control scheme is proposed to suppress the circulating currents. Through graphics, the generation mechanism of circulating currents among IPOP SDACs is qualitatively analyzed in [17] and [18]. Then, a simplified PWM with switching constraint method applied in a centralized manner is proposed to suppress the circulating currents. But the method requires that the line impedances are matched with each other. In [19], the method is expanded into a decentralized manner, then the cost of parallel converters system can be reduced. However, for these literatures, the analysis about the generation mechanism of circulating currents among IPOP SDACs lacks of detailed quantitative analysis; hence, the influence factors are not explained clearly, which limits potential and more effective control methods.

For the IPOP active-power filters (namely, TDACs), Asiminoaei *et al.* [5] minimize the circulating currents by installing common-mode inductors on each active-power filter. This approach cannot be popularized, particularly for high power, the leakage inductance may saturate the core much faster. In [6], the grid-connected dc microgrid is connected to the utility through multiple IPOP TDACs to exchange large power flow. There will be great dc offsets of currents among these IPOP TDACs, a dc droop plus 0-axis control method is designed to realize the power sharing and to eliminate dc offsets. Then, the circulating currents can be effectively suppressed. But the influence factors are not analyzed comprehensively and carefully. Compared to input-separated output-parallel TDACs, the zero-sequence circulating currents among IPOP TDACs are prominent. The zero-sequence circulating currents models among two IPOP TDACs are derived, and it is found that they are related to the zero vectors of space-vector modulation in [20]–[22]. Through adjusting the zero vectors, the zero-sequence circulating currents can be reduced. In [23], both cross-circulating-current and zero-sequence circulating-current are considered and added into the conventional droop plus virtual impedance control. Then, average current-sharing performance among parallel voltage source inverter (VSIs) can be improved. The circulating currents models are generalized to N ($N > 2$) IPOP TDACs in [24]–[27]. The circulating currents are modeled based on zero sequence, positive sequence, and negative sequence, and a corresponding suppression strategy is designed in [24], but the computation burden is very heavy. Zhang *et al.* [25] show that the circulating currents are not only susceptible to the mismatches of circuit parameters but also influenced by the interactions of circulating currents controllers used by other paralleled TDACs. Based on the analysis, a zero-vector feedforward method with space-vector modulation is proposed to suppress the circulating currents. A zero-sequence circulating currents suppression

method is introduced using carrier phase-shift pulsewidth modulation (PWM) in [26], which can reduce the peak value of zero-sequence circulating currents regardless of the number of IPOP converters. Wang *et al.* [27] analyze the circulating-current paths in the parallel system and proposes a centralized control strategy composed of the sum control and difference control to eliminate the circulating currents. Similarly, these literatures lack the detailed and strict mathematic model of circulating currents, also the related influence factors are not well studied, both of which will limit potential and more effective suppression strategies.

As narrated earlier, the studies about circulating currents are very diverse especially for many different kinds of IPOP converters in hybrid ac/dc distribution networks. Furthermore, the detailed mathematic model and corresponding characteristics of circulating currents are not well studied systematically, which will limit potential and more effective suppression strategies. Especially for the IPOP nonisolated converters, the related works are even less. But considering the economy and energy efficiency of hybrid ac/dc distribution networks, the IPOP nonisolated converters are more competitive with their high efficiency and high power density. Therefore, this paper systematically analyzes circulating currents of these heterogeneous converters, including IPOP nonisolated BDDCs, IPOP nonisolated SDACs, and IPOP nonisolated TDACs, which are the main power converters in hybrid ac/dc distribution networks. For these heterogeneous IPOP converters, a unified modeling approach is proposed to deduce the detailed mathematic models of circulating currents among different IPOP converters according to similar steps, which will make the modeling more orderly and distinctly. Based on these mathematic models, the complicated characteristics and the generation mechanism of circulating currents are clearly explained, which shows that there are various types of circulating currents including circulating currents within the single converter and circulating currents among the multiple converters. At the same time, corresponding influence factors, like line impedances, filters, and so on, are analyzed. Especially for the IPOP SDACs, the asymmetry of positive and negative input line resistances will result in instability. In addition, it is concluded that the circulating currents will cause port degradation of the converter, that is, the positive currents and the negative currents of output port or input port are not equal, which is never emphasized in existing literatures. The port degradation will make some port-based control methods ineffective and influence the relay protection, which affects the system greatly. Then, through comparison and theoretical derivation, it is found that many traditional control methods, like droop control aiming to eliminate circulating currents among input-separated output-parallel converters, are no more suitable for IPOP converters. To some extent, for the specific topologies, all types of circulating currents cannot be completely eliminated together. We hope that these essential works can make contributions to more effective suppression strategies of circulating currents among IPOP nonisolated converters. All the theoretical analyses are verified by the real-time hardware-in-loop (HIL) tests mainly composed of the RTLAB and STM32F407 MCUs.

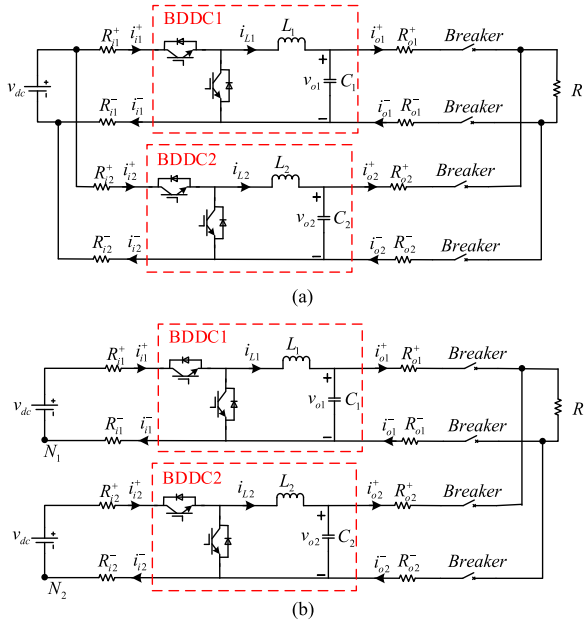

Fig. 2. Structures of two BDDCs connected in (a) the IPOP form and (b) the ISOP form.

The remainder of this paper is organized as follows. In Sections II, III, and IV, the circulating currents among IPOP nonisolated BDDCs, IPOP nonisolated SDACs, and IPOP nonisolated TDACs are systematically modeled and analyzed, respectively. In Section V, the validity of the analyses is demonstrated through HIL tests. At last, the conclusions are drawn in Section VI.

II. Circulating Currents Among IPOP Nonisolated BDDCs

A. Modeling

The BDDCs are used to convert dc voltage levels for various applications. There are different topologies of BDDCs, but this section mainly focuses on typical nonisolated BDDCs, which are widely used in practice for their simple and low-cost constructions. For convenience, we illustrate related problems through two IPOP BDDCs, but the methods and conclusions can be extended to N ($N > 2$) IPOP BDDCs with more complicated expressions.

The structure of two IPOP BDDCs is shown in Fig. 2(a). The two BDDCs operate in coordination to provide power for the load R. The outputs of BDDCs are filtered by LC filters whose inductances are L_1 and L_2 and capacitances are C_1 and C_2, respectively. The input voltage is $v_{\rm dc}$. Because in the low-voltage distribution network, the lines are mainly resistive, only the line resistances are taken into consideration. The positive input line resistances are R_{i1}^{+} and R_{i2}^{+}, respectively, while the negative input line resistances are R_{i1}^{-} and R_{i2}^{-}, respectively. The positive output line resistances are R_{o1}^{+} and R_{o2}^{+}, respectively, while the negative output line resistances are R_{o1}^{-} and R_{o2}^{-}, respectively. The breakers of positive and negative poles are used to protect the BDDCs from faults like overcurrent and so on. Fig. 2(b) shows the structure of two input-separated output-parallel (ISOP) BDDCs, the

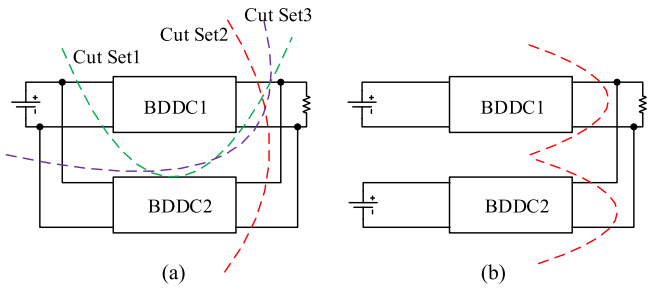

Fig. 3. Differences between IPOP BDDCs and ISOP BDDCs. (a) Currents coupling of IPOP BDDCs. (b) Currents decoupling of ISOP BDDCs.

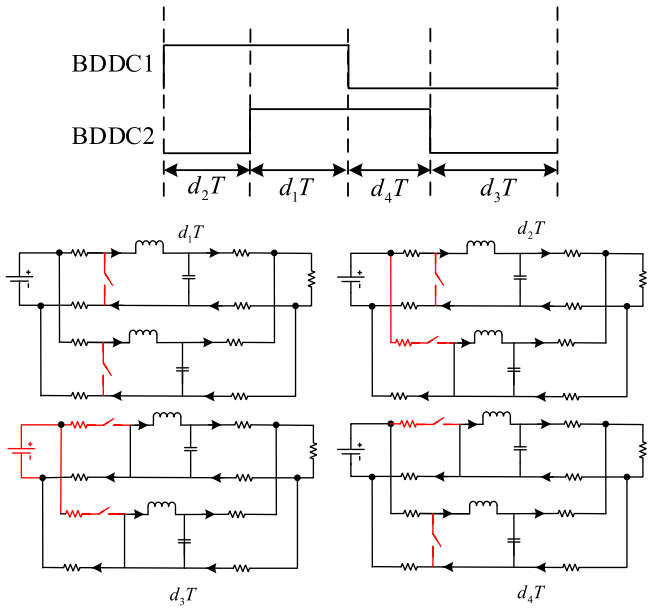

Fig. 4. Operating stages of two IPOP BDDCs.

meanings of corresponding notations are the same as those in Fig. 2(a). The ISOP structures are widely applied in microgrids to make different RESs integrate into the power system. Comparing Fig. 2(a) with Fig. 2(b), the essential difference between IPOP BDDCs and ISOP BDDCs is that the potentials of points N_1 and N_2 are clamped in IPOP BDDCs, which makes the model of IPOP BDDCs totally different from that of ISOP BDDCs.

Unlike ISOP BDDCs, the currents of IPOP BDDCs are coupled together. As Fig. 3(a) shows, according to Kirchhoff's laws, the sum of output currents and input currents of cut set1 is zero, that is, $i_{o1}^{+}-i_{o1}^{-}=i_{i1}^{+}-i_{i1}^{-}$, which cannot represent $i_{o1}^{+}-i_{o1}^{-}=0$. Through the analyses of cut set2 and cut set3, the similar conclusions can be obtained, that is, the positive currents are not always equal to the negative currents, which is called port degradation in this paper. But for the ISOP BDDCs, the positive currents are always equal to the negative currents, which can be obviously verified through the cut sets in Fig. 3(b). Because of the port degradation, the model of IPOP BDDCs becomes more complicated compared to that of ISOP BDDCs and there will be multiple types of circulating currents.

As Fig. 4 shows, there are four operating stages of two IPOP BDDCs according to the on–off states of BDDC1 and BDDC2 (omitting dead time). Based on Figs. 2(a) and 4, the average model of switch cycle can be derived as

$$\begin{cases}(d_1+d_2)\,i_{L1}R_{i1}^{+}+(d_1+d_2)\left(C_1\frac{dv_{o1}}{dt}+i_{o1}^{-}\right)R_{i1}^{-}\\ \quad+L_1\frac{di_{L1}}{dt}+v_{o1}=(d_1+d_2)\,v_{\rm dc}\\ v_{o1}-i_{o1}^{+}R_{o1}^{+}-\left(i_{o1}^{+}+i_{o2}^{+}\right)R-i_{o1}^{-}R_{o1}^{-}=0\\ (d_1+d_4)\,i_{L2}R_{i2}^{+}+(d_1+d_4)\left(C_2\frac{dv_{o2}}{dt}+i_{o2}^{-}\right)R_{i2}^{-}\\ \quad+L_2\frac{di_{L2}}{dt}+v_{o2}=(d_1+d_4)\,v_{\rm dc}\\ v_{o2}-i_{o2}^{+}R_{o2}^{+}-\left(i_{o1}^{+}+i_{o2}^{+}\right)R-i_{o2}^{-}R_{o2}^{-}=0\\ i_{o1}^{+}+i_{o2}^{+}=i_{o1}^{-}+i_{o2}^{-}\\ \left[C_1\frac{dv_{o1}}{dt}+i_{o1}^{-}-(d_3+d_4)\,i_{L1}\right]R_{i1}^{-}+i_{o1}^{-}R_{o1}^{-}\\ =\left[C_2\frac{dv_{o2}}{dt}+i_{o2}^{-}-(d_2+d_3)\,i_{L2}\right]R_{i2}^{-}+i_{o2}^{-}R_{o2}^{-}\\ i_{o1}^{+}=i_{L1}-C_1\frac{dv_{o1}}{dt},\quad i_{o2}^{+}=i_{L2}-C_2\frac{dv_{o2}}{dt}.\end{cases}\tag{1}$$

For the two ISOP BDDCs, based on Fig. 2(b) and considering the conditions that $i_{o,k}^{+}=i_{o,k}^{-}$ $(k=1,\ 2)$, the average model of switch cycle can be derived as

$$\begin{cases}(d_1+d_2)\,i_{L1}\left(R_{i1}^{+}+R_{i1}^{-}\right)+L_1\frac{di_{L1}}{dt}+v_{o1}=(d_1+d_2)\,v_{\rm dc}\\ v_{o1}-i_{o1}^{+}\left(R_{o1}^{+}+R_{o1}^{-}\right)-\left(i_{o1}^{+}+i_{o2}^{+}\right)R=0\\ (d_1+d_4)\,i_{L2}\left(R_{i2}^{+}+R_{i2}^{-}\right)+L_2\frac{di_{L2}}{dt}+v_{o2}=(d_1+d_4)\,v_{\rm dc}\\ v_{o2}-i_{o2}^{+}\left(R_{o2}^{+}+R_{o2}^{-}\right)-\left(i_{o1}^{+}+i_{o2}^{+}\right)R=0\\ i_{o1}^{+}=i_{L1}-C_1\frac{dv_{o1}}{dt},\quad i_{o2}^{+}=i_{L2}-C_2\frac{dv_{o2}}{dt}.\end{cases}\tag{2}$$

Comparing (1) and (2), it can be found that the model of two IPOP BDDCs is more complicated than the model of two ISOP BDDCs. Furthermore, through observation, it can be concluded that for ISOP BDDCs, the line resistances of positive poles and negative poles can be combined together, that is, their effects are equal to the resistance $R_{i,k}^{+}+R_{i,k}^{-}$ or $R_{o,k}^{+}+R_{o,k}^{-}$ $(k=1,\ 2)$. But for IPOP BDDCs, the line resistances of positive poles and negative poles must be considered separately.

B. Analysis

This section mainly studies the steady state of IPOP BDDCs according to (1) and reveals the corresponding influence factors about circulating currents. Let the differential terms of (1) equal to zero and simplify the unknown variables, the steady state equations can be gotten as follows.

The steady values of output currents can be solved through (3) shown at the bottom of the next page, at the same time, the sensitivity analysis of related parameters like line resistances can be conducted to reveal the corresponding influence factors about circulating currents. Through (3), it can be concluded that the output line resistances, the input line resistances and duty ratios all have influences on the output currents. The influences of duty ratios are only related to individual "on" time (d_1+d_2 and d_1+d_4) or "off" time (d_3+d_4 and d_2+d_3) of BDDC1 or BDDC2. Hence, their influences are obvious and the detailed analyses about duty ratios are omitted.

Compared to duty ratios, the influences of input and output line resistances are more complicated, which need to be analyzed in detail. Since there are multiple independent variables

TABLE I
SYSTEM PARAMETERS OF IPOP BDDCS

Parameters	Rated Value
v_{dc}	1000 V
R	2 Ω
$C_1, C_2,\ L_1, L_2$	5 mF, 5 mF, 1 mH, 1mH
$d_1, d_2,\ d_3, d_4$	0.2, 0.3, 0.3, 0.2
$R_{i1}^-,\ R_{i1}^+, R_{i2}^-,\ R_{i2}^+$	0.01 Ω, 0.01 Ω, 0.01 Ω, 0.01 Ω
$R_{o1}^-,\ R_{o1}^+, R_{o2}^-,\ R_{o2}^+$	0.01 Ω, 0.01 Ω, 0.01 Ω, 0.01 Ω,

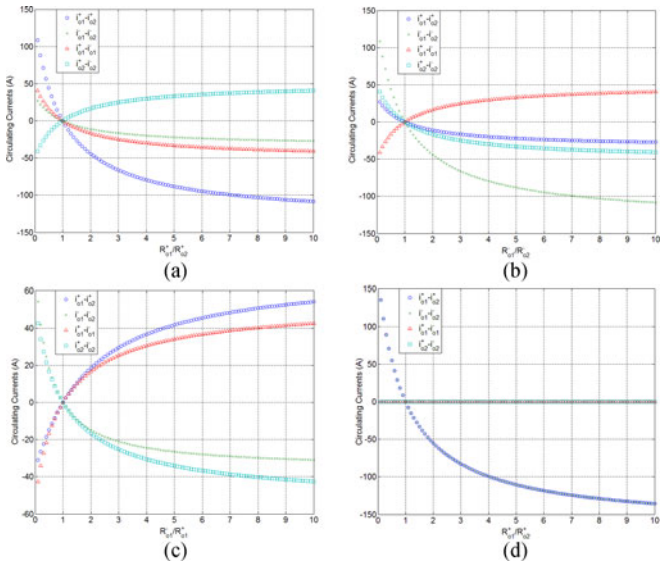

Fig. 5. Circulating currents among IPOP BDDCs with changes of output line resistances. (a) $R_{o1}^+ + R_{o2}^+ = 0.02\ \Omega$ and R_{o1}^+/R_{o2}^+ is changed. (b) $R_{o1}^- + R_{o2}^- = 0.02\ \Omega$ and R_{o1}^-/R_{o2}^- is changed. (c) $R_{o1}^+ + R_{o1}^- = 0.02\ \Omega$ and R_{o1}^-/R_{o1}^+ is changed. (d) $R_{o1}^+ + R_{o2}^+ = 0.02\ \Omega$, $R_{o1}^+ = R_{o1}^-$, $R_{o2}^+ = R_{o2}^-$, and R_{o1}^+/R_{o2}^+ is changed.

which influence the solutions as shown in (3), the expressions of analytical solutions are complicated. Therefore, the numerical solutions are used to study related problems and the rated system parameters used for numerical calculation are shown in Table I.

Fig. 5 shows the circulating currents among IPOP BDDCs with the changes of output line resistances. The circulating currents are divided into four types, that is, $i_{o1}^+ - i_{o2}^+$ (two positive poles), $i_{o1}^- - i_{o2}^-$ (two negative poles), $i_{o1}^+ - i_{o1}^-$, and $i_{o2}^+ - i_{o2}^-$ (inner circulating currents). The influence factors of output line resistance are also divided into four situations, where the other

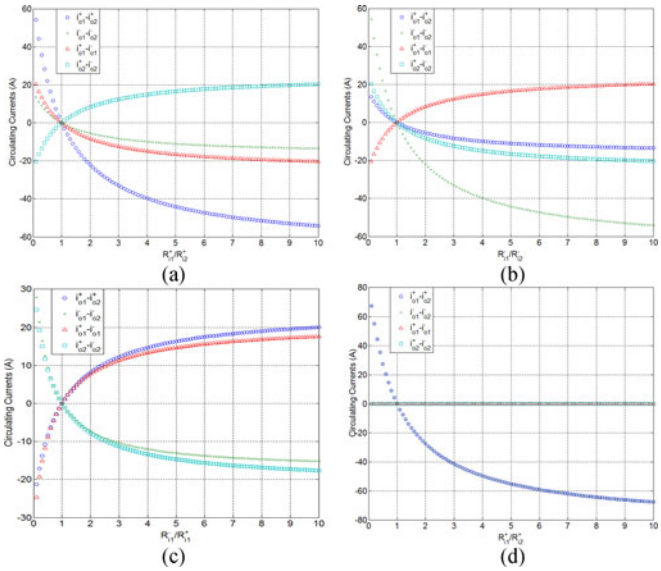

Fig. 6. Circulating currents among IPOP BDDCs with changes of input line resistances. (a) $R_{i1}^+ + R_{i2}^+ = 0.02\ \Omega$ and R_{i1}^+/R_{i2}^+ is changed. (b) $R_{i1}^- + R_{i2}^- = 0.02\ \Omega$ and R_{i1}^-/R_{i2}^- is changed. (c) $R_{i1}^+ + R_{i1}^- = 0.02\ \Omega$ and R_{i1}^-/R_{i1}^+ is changed. (d)$R_{i1}^+ + R_{i2}^+ = 0.02\ \Omega$, $R_{i1}^+ = R_{i1}^-$, $R_{i2}^+ = R_{i2}^-$, and R_{i1}^+/R_{i2}^+ is changed.

parameters are kept the same as Table I except the variable parameters. Fig. 5(a) shows the circulating currents when the differences of two positive output line resistances are changed, where $R_{o1}^+ + R_{o2}^+ = 0.02\ \Omega$ but their ratio R_{o1}^+/R_{o2}^+ is changed. As a contrast, Fig. 5(b) shows the circulating currents when the differences of two negative output line resistances are changed, where $R_{o1}^- + R_{o2}^- = 0.02\ \Omega$ but their ratio R_{o1}^-/R_{o2}^- is changed. Fig. 5(c) shows the circulating currents when the differences of positive and negative output line resistances in BDDC1 are changed, where $R_{o1}^+ + R_{o1}^- = 0.02\ \Omega$, but their ratio R_{o1}^-/R_{o1}^+ is changed. Fig. 5(d) shows the circulating currents when the positive and negative output line resistances of individual BDDC are kept the same, respectively, but output line resistances of different BDDCs are changed, where $R_{o1}^+ = R_{o1}^-$, $R_{o2}^+ = R_{o2}^-$, $R_{o1}^+ + R_{o2}^+ = 0.02\ \Omega$, but the ratio R_{o1}^+/R_{o2}^+ is changed. The influences of input line resistances are studied in similar ways, which are shown in Fig. 6.

From Figs. 5 and 6, it can be seen that both the input and output line resistances have influences on circulating currents, but the sensitivity is not different. The differences of output line resistances have greater influences on circulating currents

$$\begin{bmatrix} (d_1+d_2)\,R_{i1}^+ + R_{o1}^+ + R & R & (d_1+d_2)\,R_{i1}^- + R_{o1}^- & 0 \\ R & (d_1+d_4)\,R_{i2}^+ + R_{o2}^+ + R & 0 & (d_1+d_4)\,R_{i2}^- + R_{o2}^- \\ 1 & 1 & -1 & -1 \\ -(d_3+d_4)\,R_{i1}^- & (d_2+d_3)\,R_{i2}^- & R_{i1}^- + R_{o1}^- & -\left(R_{i2}^- + R_{o2}^-\right) \end{bmatrix} \cdot \begin{bmatrix} i_{o1}^+ \\ i_{o2}^+ \\ i_{o1}^- \\ i_{o2}^- \end{bmatrix} = \begin{bmatrix} (d_1+d_2)\,v_{\mathrm{dc}} \\ (d_1+d_4)\,v_{\mathrm{dc}} \\ 0 \\ 0 \end{bmatrix} \tag{3}$$

compared to the input line resistances. At the same time, the changes of different parameters have different influences on various circulating currents. Like the differences of two positive line resistances influence the circulating currents between two positive poles greatly, that is, $i_{o1}^{+}-i_{o2}^{+}$ changes significantly with the changes of R_{o1}^{+}/R_{o2}^{+} or R_{i1}^{+}/R_{i2}^{+}, as Figs. 5(a) and 6(a) show. The similar relationship can be found between $i_{o1}^{-}-i_{o2}^{-}$ and R_{o1}^{-}/R_{o2}^{-} or R_{i1}^{-}/R_{i2}^{-}, as Figs. 5(b) and 6(b) show. Compared to ISOP BDDCs, the biggest difference is that the circulating currents still exist even though $R_{o1}^{+}+R_{o1}^{-}=R_{o2}^{+}+R_{o2}^{-}$ and $R_{i1}^{+}+R_{i1}^{-}=R_{i2}^{+}+R_{i2}^{-}$, as Figs. 5(c) and 6(c) show. If both the positive and negative line resistances of individual BDDC can be kept the same, then there are no inner circulating currents in the BDDC, as Figs. 5(d) and 6(d) show.

On the other hand, it can be seen that the port degradation is obvious, that is, $i_{o1}^{+}-i_{o1}^{-}\neq 0$ or $i_{o2}^{+}-i_{o2}^{-}\neq 0$. The port degradation will make some port-based control methods ineffective [28]–[31]. Taking the impedance analysis as an example, because the output currents of positive and negative poles are different, the concept of "impedance" is hard to define in the dc system. Therefore, the impedance analysis will be challenged and needs to extend. Furthermore, the port degradation will influence relay protection. Usually, the breakers of the positive and the negative poles are set the same protection values. If the port degradation is not considered, the breakers will act frequently because of the great differences between the positive and negative currents.

The conventional droop control applied to ISOP BDDCs cannot suppress the circulating currents among IPOP BDDCs effectively. Assuming the droop control using the positive currents i_{o1}^{+} and i_{o2}^{+} as feedback signals, then the equivalent control effects of droop control can be thought that two same resistances, namely, the droop coefficients ($\gg$ positive output line resistances) are added to the positive poles to make the equivalent positive output line resistance equal. But for the IPOP BDDCs, even though the positive output line resistances are the same, the circulating currents can still exist as shown in Figs. 5(b) and 6(b). That is, the conventional droop control cannot suppress the circulating currents among IPOP BDDCs effectively.

Also, through the steady state equations, the corresponding inverse problem can be illustrated. That is, whether there are duty ratios to eliminate circulating currents. Assume the existing duty ratios that can eliminate circulating currents and then let $i_{o1}^{+}=i_{o1}^{-}=i_{o2}^{+}=i_{o2}^{-}=I$. The following steady-state equations can be derived according to (1):

$$\begin{cases}\left[(d_1+d_2)\left(R_{i1}^{+}+R_{i1}^{-}\right)+R_{o1}^{+}+R_{o1}^{-}+2R\right]I=(d_1+d_2)\,v_{\mathrm{dc}}\\ \left[(d_1+d_4)\left(R_{i2}^{+}+R_{i2}^{-}\right)+R_{o2}^{+}+R_{o2}^{-}+2R\right]I=(d_1+d_4)\,v_{\mathrm{dc}}\\ (d_1+d_2)\,R_{i1}^{-}+R_{o1}^{-}=(d_1+d_4)\,R_{i2}^{-}+R_{o2}^{-}\end{cases}\tag{4}$$

Equation (4) cannot hold unless $\frac{R_{o1}^{+}+R_{o1}^{-}+2R}{v_{\mathrm{dc}}/I-(R_{i1}^{+}+R_{i1}^{-})}R_{i1}^{-}+R_{o1}^{-}=\frac{R_{o2}^{+}+R_{o2}^{-}+2R}{v_{\mathrm{dc}}/I-(R_{i2}^{+}+R_{i2}^{-})}R_{i2}^{-}+R_{o2}^{-}$. This condition does not always hold for arbitrary I. Therefore, for the general cases, all types of circulating currents among IPOP BDDCs cannot be eliminated completely and only specific types of circulating currents can be eliminated, like that the droop control can suppress the circulating currents between two positive poles.

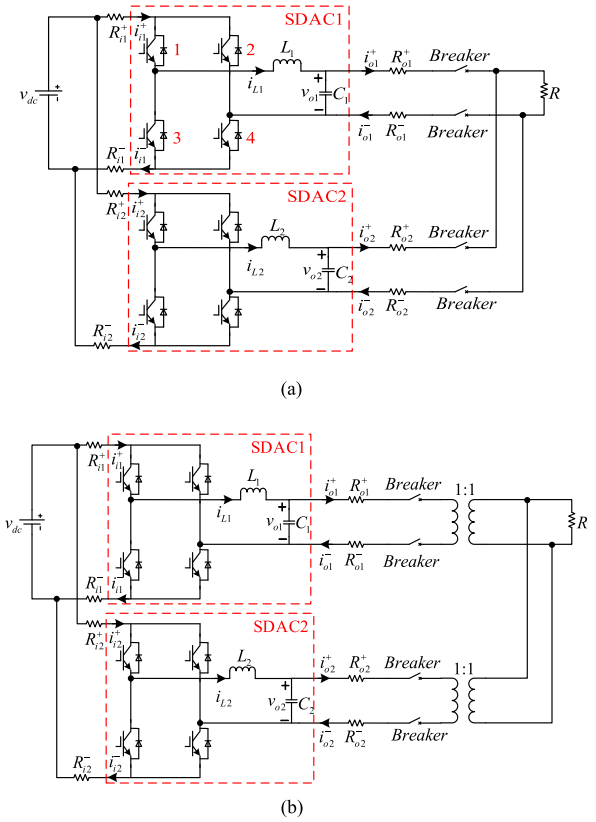

Fig. 7. Structures of two SDACs connected in (a) the IPOP form and (b) the IPOS form.

III. Circulating Currents among IPOP Nonisolated SDACs

A. Modeling

The SDACs are used to realize the mutual conversion between ac power and dc power for the low-voltage residential power. The topologies of BDDCs are various for different application. This section mainly focuses on typical nonisolated H-bridge SDACs, which are widely used in practice with their simple and low-cost constructions. For convenience, we illustrate related problems through two IPOP SDACs, but the methods and conclusions can be extended to N ($N>2$) IPOP SDACs with more complicated expressions.

The structure of two IPOP SDACs is shown in Fig. 7(a). The two SDACs operate in coordination to provide power for the load R. The outputs of SDACs are filtered by LC filters whose inductances are L_1 and L_2, capacitances are C_1 and C_2, respectively. The input voltage is v_{dc}. Because in the low-voltage distribution network, the lines are mainly resistive, only the line resistances are taken into consideration. The positive input line resistances are R_{i1}^{+} and R_{i2}^{+}, respectively, while the negative input line resistances are R_{i1}^{-} and R_{i2}^{-}, respectively. The positive output line resistances are R_{o1}^{+} and R_{o2}^{+}, respectively, while the negative output line resistances are R_{o1}^{-} and R_{o2}^{-}, respectively. The breakers

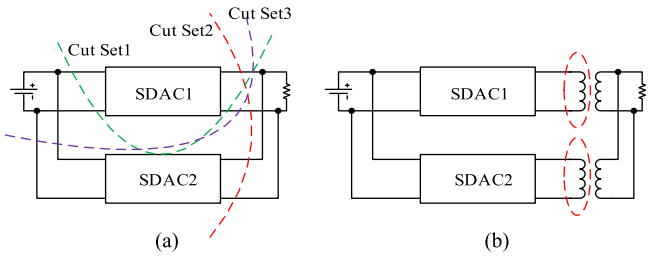

Fig. 8. Differences between IPOP SDACs and IPOS SDACs. (a) Currents coupling of IPOP SDACs. (b) Currents decoupling of IPOS SDACs.

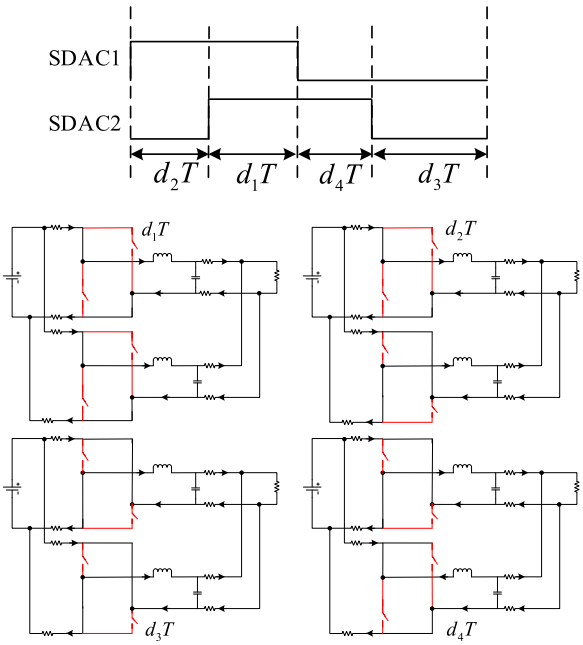

Fig.9. Operating stages of two IPOP SDACs.

of positive and negative poles are used to protect the SDACs from faults. Fig. 7(b) shows the structure of two input-parallel output-separated (IPOS) SDACs with an isolation transformer in the output terminal, the meanings of corresponding notations are the same as those in the Fig. 7(a).

Being similar to the analysis of IPOP BDDCs, the currents of IPOP SDACs are coupled together too as shown in Fig. 8(a). That is, the port degradation also occurs in the IPOP SDACs. On the other hand, the currents of IPOS SDACs are simple and decoupled, the positive currents are always equal to the negative currents, which is similar to the ISOP BDDCs and can be obviously verified through the cut sets in Fig. 8(b). Due to the port degradation, the model of IPOP SDACs becomes more complex and there will be multiple types of circulating currents.

The unified modeling approach is used to establish the model of circulating currents among IPOP SDACs, which has been adopted in the modeling of circulating currents among nonisolated IPOP BDDCs. According to the on–off states of SDAC1 and SDAC2 based on bipolar modulation ($d = 1$, Tube1 and Tube4 are on; $d = 0$, Tube2 and Tube3 are on), there are four operating stages (omitting dead time) of two IPOP SDACs, as shown in Fig. 9. Based on Figs. 7(a) and 9, the average model of switch cycle can be derived as

$$\begin{cases} L_1\frac{di_{L1}}{dt} + i_{L1}\left[(d_1+d_2)R_{i1}^{+} + (d_3+d_4)R_{i1}^{-}\right] + v_{o1} \\ \quad + \left(C_1\frac{dv_{o1}}{dt} + i_{o1}^{-}\right)\left[(d_1+d_2)R_{i1}^{-} + (d_3+d_4)R_{i1}^{+}\right] \\ \quad = (d_1+d_2-d_3-d_4)\,v_{\rm dc} \\ v_{o1} - i_{o1}^{+}R_{o1}^{+} - \left(i_{o1}^{+}+i_{o2}^{+}\right)R - i_{o1}^{-}R_{o1}^{-} = 0 \\ L_2\frac{di_{L2}}{dt} + i_{L2}\left[(d_1+d_4)R_{i2}^{+} + (d_2+d_3)R_{i2}^{-}\right] + v_{o2} \\ \quad + \left(C_2\frac{dv_{o2}}{dt} + i_{o2}^{-}\right)\left[(d_1+d_4)R_{i2}^{-} + (d_2+d_3)R_{i2}^{+}\right] \\ \quad = (d_1+d_4-d_2-d_3)\,v_{\rm dc} \\ v_{o2} - i_{o2}^{+}R_{o2}^{+} - \left(i_{o1}^{+}+i_{o2}^{+}\right)R - i_{o2}^{-}R_{o2}^{-} = 0 \\ i_{o1}^{+} + i_{o2}^{+} = i_{o1}^{-} + i_{o2}^{-} \\ \left(C_1\frac{dv_{o1}}{dt} + i_{o1}^{-}\right)\left[(d_1+d_2)R_{i1}^{-} + (d_3+d_4)R_{i1}^{+}\right] \\ \quad + i_{o1}^{-}R_{o1}^{-} + d_4 v_{\rm dc} \\ = \left(C_2\frac{dv_{o2}}{dt} + i_{o2}^{-}\right)\left[(d_1+d_4)R_{i2}^{-} + (d_2+d_3)R_{i2}^{+}\right] \\ \quad + i_{o2}^{-}R_{o2}^{-} + d_2 v_{\rm dc} \\ i_{o1}^{+} = i_{L1} - C_1\frac{dv_{o1}}{dt},\quad i_{o2}^{+} = i_{L2} - C_2\frac{dv_{o2}}{dt}. \end{cases} \tag{5}$$

For the two IPOS SDACs, based on Fig. 7(b) and considering the conditions that $i_{o,k}^{+} = i_{o,k}^{-}$ $(k = 1,\ 2)$, the average model of switch cycle can be derived as

$$\begin{cases} L_1\frac{di_{L1}}{dt} + i_{L1}\left(R_{i1}^{+} + R_{i1}^{-}\right) + v_{o1} = (d_1+d_2-d_3-d_4)\,v_{\rm dc} \\ v_o1 - i_o1^{+}(R_o1^{+} + R_o1^{-}) - (i_o1^{+} + i_o2^{+})R = 0 \\ L_2\frac{di_{L2}}{dt} + i_{L2}\left(R_{i2}^{+} + R_{i2}^{-}\right) + v_{o2} = (d_1+d_4-d_2-d_3)\,v_{\rm dc} \\ v_{o2} - i_{o2}^{+}\left(R_{o2}^{+} + R_{o2}^{-}\right) - \left(i_{o1}^{+} + i_{o2}^{+}\right)R = 0 \\ i_{o1}^{+} = i_{L1} - C_1\frac{dv_{o1}}{dt},\quad i_{o2}^{+} = i_{L2} - C_2\frac{dv_{o2}}{dt}. \end{cases} \tag{6}$$

Comparing (5) and (6), it can be found that the model of two IPOP SDACs is more complicated than the model of two IPOS SDACs. Furthermore, through observation, it can be concluded that for IPOS SDACs, the line resistances of positive poles and negative poles can be combined together, that is, their effects are equal to the resistance $R_{i,k}^{+} + R_{i,k}^{-}$ or $R_{o,k}^{+} + R_{o,k}^{-} (k = 1,\ 2)$. But for IPOP SDACs, the line resistances of positive poles and negative poles must be considered separately. These conclusions are similar to those of IPOP BDDCs and ISOP BDDCs.

B. Analysis

This part mainly studies the steady state of IPOP SDACs according to (5) and reveals the corresponding influence factors about circulating currents. Compared to dc steady solutions of IPOP BDDCs, the steady solutions of (5) are more complex because of the ac variables. For simplification and mainly studying the influences of line resistances, duty ratios of SDAC1 and SDAC2 are assumed to be the same. That is, $d_1 + d_2 = d_1 + d_4 = 0.5 + D \cdot \sin(\omega t)$, and then $d_3 + d_4 = d_2 + d_3 = 0.5 - D \cdot \sin(\omega t)$.

Let $i_{L,k} = I_{L,k}^{s}\sin(\omega t) + I_{L,k}^{c}\cos(\omega t)$, $v_{o,k} = V_{o,k}^{s}\sin(\omega t) + V_{o,k}^{c}\cos(\omega t)$, $i_{o,k}^{+} = I_{o,k}^{+s}\sin(\omega t) + I_{o,k}^{+c}\cos(\omega t)$, $i_{o,k}^{-} = I_{o,k}^{-s}\sin(\omega t) + I_{o,k}^{-c}\cos(\omega t), k = 1,\ 2$. The steady-state equations can

be gotten as follows:

$$\begin{aligned}&\left[\omega L_k I^s_{L,k} + 0.5\left(R^+_{i,k} + R^-_{i,k}\right) I^c_{L,k} + 0.5\omega C_k\left(R^+_{i,k} + R^-_{i,k}\right) V^s_{o,k}\right.\\&\left. + 0.5\left(R^+_{i,k} + R^-_{i,k}\right) I^{-c}_{o,k} + V^c_{o,k}\right]\cos(\omega t) + \left[-\omega L_k I^c_{L,k}\right.\\&\left. + 0.5\left(R^+_{i,k} + R^-_{i,k}\right) I^s_{L,k} - 0.5\omega C_k\left(R^+_{i,k} + R^-_{i,k}\right) V^c_{o,k}\right.\\&\left. + 0.5\left(R^+_{i,k} + R^-_{i,k}\right) I^{-s}_{o,k} + V^s_{o,k} - 2Dv_{dc}\right]\sin(\omega t)\\&+ \left(\mathbf{DI^s_{L,k} + \omega C_k DV^c_{o,k} - DI^{-s}_{o,k}}\right)\left(\boldsymbol{R^+_{i,k} - R^-_{i,k}}\right)\mathbf{\sin(\omega t)\sin(\omega t)}\\&+ \left(\mathbf{DI^c_{L,k} - \omega C_k DV^s_{o,k} - DI^{-c}_{o,k}}\right)\left(\boldsymbol{R^+_{i,k} - R^-_{i,k}}\right)\mathbf{\sin(\omega t)\cos(\omega t)}\\&= 0 \qquad (7)\end{aligned}$$

$$\begin{aligned}&\left[V^c_{o,k} - R^+_{o,k} I^{+c}_{o,k} - R\left(I^{+c}_{o1} + I^{+c}_{o2}\right) - R^-_{o,k} I^{-c}_{o,k}\right]\cos(\omega t)\\&+ \left[V^s_{o,k} - R^+_{o,k} I^{+s}_{o,k} - R\left(I^{+s}_{o1} + I^{+s}_{o2}\right) - R^-_{o,k} I^{-s}_{o,k}\right]\sin(\omega t) = 0\end{aligned} \qquad (8)$$

$$\begin{aligned}&\left(I^{+c}_{o,k} - I^c_{L,k} + \omega C_k V^s_{o,k}\right)\cos(\omega t)\\&\quad + \left(I^{+s}_{o,k} - I^s_{L,k} - \omega C_k V^c_{o,k}\right)\sin(\omega t) = 0\end{aligned} \qquad (9)$$

$$\begin{aligned}&\left(I^{+c}_{o1} + I^{+c}_{o2} - I^{-c}_{o1} - I^{-c}_{o2}\right)\cos(\omega t)\\&\quad + \left(I^{+s}_{o1} + I^{+s}_{o2} - I^{-s}_{o1} - I^{-s}_{o2}\right)\sin(\omega t) = 0\end{aligned} \qquad (10)$$

$$\begin{aligned}&\left[0.5\omega C_1\left(R^+_{i1} + R^-_{i1}\right) V^s_{o1} + \left(R^-_{o1} + 0.5R^+_{i1} + 0.5R^-_{i1}\right) I^{-c}_{o1}\right.\\&\left. - 0.5\omega C_2\left(R^+_{i2} + R^-_{i2}\right) V^s_{o2} - \left(R^-_{o2} + 0.5R^+_{i2} + 0.5R^-_{i2}\right) I^{-c}_{o2}\right]\\&\times\cos(\omega t) + \left[-0.5\omega C_1\left(R^+_{i1} + R^-_{i1}\right) V^c_{o1}\right.\\&\left. + \left(R^-_{o1} + 0.5R^+_{i1} + 0.5R^-_{i1}\right) I^{-s}_{o1} + 0.5\omega C_2\left(R^+_{i2} + R^-_{i2}\right) V^c_{o2}\right.\\&\left. - \left(R^-_{o2} + 0.5R^+_{i2} + 0.5R^-_{i2}\right) I^{-s}_{o2}\right]\sin(\omega t)\\&+ \left[\left(\boldsymbol{\omega C_1 DV^c_{o1} - DI^{-s}_{o1}}\right)\left(\boldsymbol{R^+_{i1} - R^-_{i1}}\right) - \left(\boldsymbol{\omega C_2 DV^c_{o2} - DI^{-s}_{o2}}\right)\right.\\&\left.\times\left(\boldsymbol{R^+_{i2} - R^-_{i2}}\right)\right]\mathbf{\sin(\omega t)\sin(\omega t)}\\&+ \left[\left(\boldsymbol{-\omega C_1 DV^s_{o1} - DI^{-c}_{o1}}\right)\left(\boldsymbol{R^+_{i1} - R^-_{i1}}\right) + \left(\boldsymbol{\omega C_2 DV^s_{o2} + DI^{-c}_{o2}}\right)\right.\\&\left.\times\left(\boldsymbol{R_{i2}{}^+ - R^-_{i2}}\right)\right]\mathbf{\sin(\omega t)\cos(\omega t)} = 0.\end{aligned} \qquad (11)$$

The unknown variables $I^{+s}_{o,k}$, $I^{+c}_{o,k}$, $I^{-s}_{o,k}$, $I^{-c}_{o,k}$, and so on, can be solved through letting the coefficients of trigonometric functions equal to zero in (7)–(11), then the steady values of output currents can be obtained based on $I^{+s}_{o,k}$, $I^{+c}_{o,k}$, $I^{-s}_{o,k}$, and $I^{-c}_{o,k}$. At the same time, the sensitivity analysis of related parameters like line resistances can be conducted to reveal the corresponding influence factors about circulating currents.

Equations (7) and (11) contain more than two constraints, as emphasized in bold font, that is,

$$\begin{cases}\left(DI^s_{L,k} + \omega C_k DV^c_{o,k} - DI^{-s}_{o,k}\right)\left(R^+_{i,k} - R^-_{i,k}\right) = 0\\ \left(DI^c_{L,k} - \omega C_k DV^s_{o,k} - DI^{-c}_{o,k}\right)\left(R^+_{i,k} - R^-_{i,k}\right) = 0\\ \left(\omega C_1 DV^c_{o1} - DI^{-s}_{o1}\right)\left(R^+_{i1} - R^-_{i1}\right)\\ \quad - \left(\omega C_2 DV^c_{o2} - DI^{-s}_{o2}\right)\left(R^+_{i2} - R^-_{i2}\right) = 0\\ \left(-\omega C_1 DV^s_{o1} - DI^{-c}_{o1}\right)\left(R^+_{i1} - R^-_{i1}\right)\\ \quad + \left(\omega C_2 DV^s_{o2} + DI^{-c}_{o2}\right)\left(R^+_{i2} - R^-_{i2}\right) = 0\end{cases}. \qquad (12)$$

TABLE II
SYSTEM PARAMETERS OF IPOP SDACS

Parameters	Rated Value
v_{dc}	1000 V
R	2 Ω
D, ω	0.3, 100π rad/s
C_1, C_2, L_1, L_2	8 mF, 8 mF, 1 mH, 1 mH
R^-_{i1}, R^+_{i1}, R^-_{i2}, R^+_{i2}	0.01 Ω, 0.01 Ω, 0.01 Ω, 0.01 Ω
R^-_{o1}, R^+_{o1}, R^-_{o2}, R^+_{o2}	0.01 Ω, 0.01 Ω, 0.01 Ω, 0.01 Ω

Then the total number of constraints will exceed the total number of unknown variables, which will make (7)–(11) to have no solutions in the fundamental frequency. If (7)–(11) can hold, there must be other harmonic components in $i_{L,k}$, $v_{o,k}$, $i^+_{o,k}$, and $i^-_{o,k}$. Through simulation, it can be found that the harmonics are very large so that they make the IPOP SDACs unstable. Through observing (12), if $R^+_{i,k} = R^-_{i,k}$, ($k = 1, 2$), the equations can hold, no matter what the unknown variables are. Then, the constraints of (12) can be released. Therefore, if the IPOP SDACs are stable, the necessary conditions are that $R^+_{i,k} = R^-_{i,k}$ ($k = 1, 2$). This conclusion can be easily expanded to general situations when $d_1 + d_2 \neq d_1 + d_4$. For the IPOS SDACs or ISOP SDACs, the asymmetry of positive input line resistances and negative input line resistances will not result in instability, which can be easily proved through (6). This phenomenon indicates that the IPOP SDACs are essentially different from the IPOS SDACs and ISOP SDACs.

Since (7)–(11) are pretty complex, the expressions of analytical solutions are difficult to obtain. Therefore, the numerical solutions are used to study related problems and the rated system parameters used for numerical calculation are shown in Table II.

Fig. 10 shows the circulating currents among IPOP SDACs with the changes of output line resistances. Being similar to the analysis of the circulating currents among IPOP BDDCs, the circulating currents are divided into four types, that is, $i^+_{o1} - i^+_{o2}$ (two positive poles), $i^-_{o1} - i^-_{o2}$ (two negative poles), $i^+_{o1} - i^-_{o1}$, and $i^+_{o2} - i^-_{o2}$ (inner circulating currents). The influence factors of output line resistance are divided into four situations, where the other parameters are kept the same as Table II except the variable parameters. Fig. 10(a) shows the circulating currents when the differences of two positive output line resistances are changed, where $R^+_{o1} + R^+_{o2} = 0.02\ \Omega$ but their ratio R^+_{o1}/R^+_{o2} is changed. As a contrast, Fig. 10(b) shows the circulating currents when the differences of two negative output line resistances are changed, where $R^-_{o1} + R^-_{o2} = 0.02\ \Omega$ but their ratio R^-_{o1}/R^-_{o2} is changed. Fig. 10(c) shows the circulating currents when the differences of positive and negative output line resistances in SDAC1 are changed, where $R^+_{o1} + R^-_{o1} = 0.02\ \Omega$ but their ratio R^-_{o1}/R^+_{o1} is changed. Fig. 10(d) shows the circulating currents when the positive and negative output line resistances of individual SDAC are kept the same, respectively, but the output line resistances of different SDACs are changed, where $R^+_{o1} = R^-_{o1}$, $R^+_{o2} = R^-_{o2}$, and $R^+_{o1} + R^+_{o2} = 0.02\ \Omega$ but the ratio R^+_{o1}/R^+_{o2} is changed.

Fig. 11 shows the circulating currents among IPOP SDACs with the changes of input line resistances and filters. Because the positive input line resistances and negative input line resistances

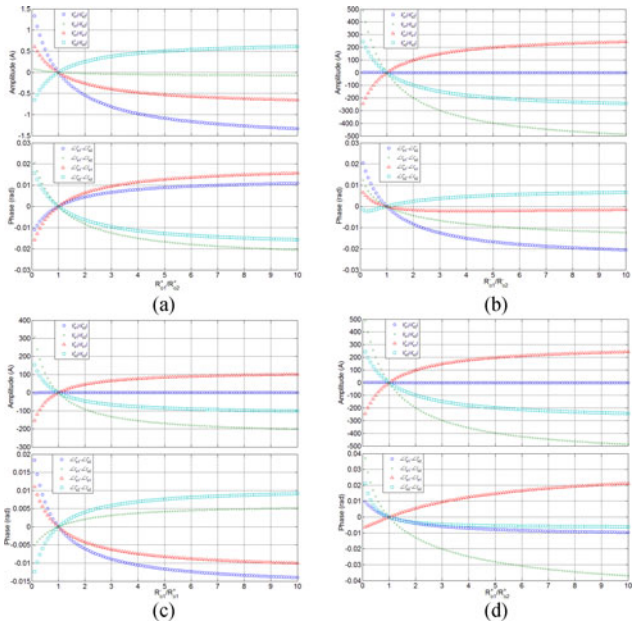

Fig. 10. Circulating currents among IPOP SDACs with changes of output line resistances. (a) $R_{o1}^{+}+R_{o2}^{+}=0.02\ \Omega$ and R_{o1}^{+}/R_{o2}^{+} is changed. (b) $R_{o1}^{-}+R_{o2}^{-}=0.02\ \Omega$ and R_{o1}^{-}/R_{o2}^{-} is changed. (c) $R_{o1}^{+}+R_{o1}^{-}=0.02\ \Omega$ and R_{o1}^{-}/R_{o1}^{+} is changed. (d) $R_{o1}^{+}+R_{o2}^{+}=0.02\ \Omega$, $R_{o1}^{+}=R_{o1}^{-}$, $R_{o2}^{+}=R_{o2}^{-}$, and R_{o1}^{+}/R_{o2}^{+} is changed.

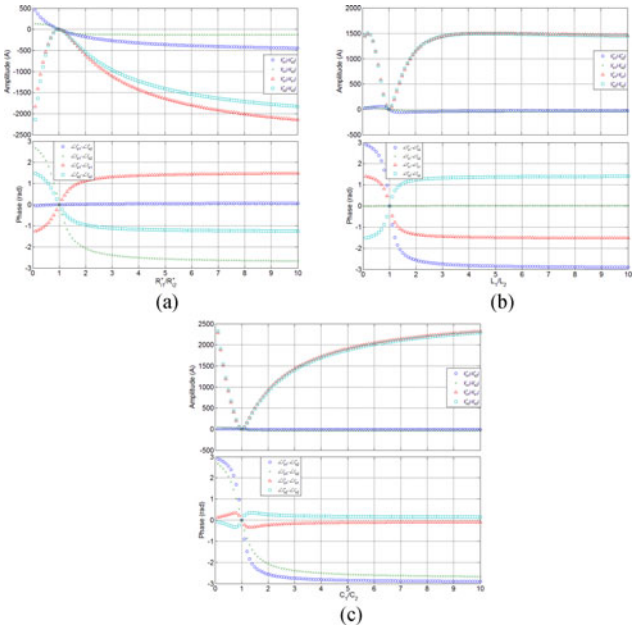

Fig. 11. Circulating currents among IPOP SDACs with changes of input line resistances and filters. (a) $R_{i1}^{+}+R_{i2}^{+}=0.02\ \Omega$, $R_{i1}^{+}=R_{i1}^{-}$, $R_{i2}^{+}=R_{i2}^{-}$, and R_{i1}^{+}/R_{i2}^{+} is changed. (b) $L_1+L_2=2$ mH and L_1/L_2 is changed. (c) $C_1+C_2=16$ mF and C_1/C_2 is changed.

must be kept the same to ensure the stability of the IPOP SDACs, we mainly research the circulating currents when the input line resistances of two SDACs are different but the positive and negative input line resistances of individual SDAC are kept the same. That is, $R_{i1}^{+}+R_{i2}^{+}=0.02\ \Omega$, $R_{i1}^{+}=R_{i1}^{-}$, $R_{i2}^{+}=R_{i2}^{-}$ but R_{i1}^{+}/R_{i2}^{+} is changed, and the other parameters are kept the same as Table II. The results are shown in Fig. 11(a). The influence of filters are shown in Fig. 11(b) and (c), where $L_1+L_2=2$ mH but L_1/L_2 is changed, $C_1+C_2=16$ mF but C_1/C_2 is changed, respectively. The other parameters are kept the same as Table II.

From Figs. 10 and 11, it can be seen that asymmetry of the input or output line resistances and filters will cause serious circulating currents among IPOP SDACs with different sensitivity. Compared to the differences of two positive line resistances, the differences of two negative line resistances have greater influences on circulating currents, as shown in Fig. 10(a) and (b). The biggest difference is that the circulating currents still exist even though $R_{o1}^{+}+R_{o1}^{-}=R_{o2}^{+}+R_{o2}^{-}$ and $R_{i1}^{+}+R_{i1}^{-}=R_{i2}^{+}+R_{i2}^{-}$, as shown in Fig. 10(c), which will not occur in IPOS SDACs. Unlike the IPOP BDDCs, even both the positive and negative line resistances of individual SDAC are kept the same, the inner circulating currents in the single SDAC still exist, as shown in Figs. 10(d) and 11(a).

On the other hand, it can be also seen that the port degradation is obvious, that is, $i_{o1}^{+}-i_{o1}^{-}\neq 0$ or $i_{o2}^{+}-i_{o2}^{-}\neq 0$. The degradation will make some port-based control methods ineffective and influence relay protection. According to the similar analysis of BDDCs, the conventional droop control applied to IPOS SDACs cannot suppress the circulating currents among IPOP SDACs effectively.

Through the steady-state equations, the corresponding inverse problem can be researched. Namely, whether there are duty ratios to eliminate circulating currents based on the bipolar modulation. Similarly, assume existing duty ratios that can eliminate circulating currents, and then let $i_{o1}^{+}=i_{o1}^{-}=i_{o2}^{+}=i_{o2}^{-}=i$, $d_1+d_2=0.5+d_a$, $d_1+d_4=0.5+d_b$. With the aforementioned analysis that if IPOP SDACs are stable, then $R_{i,k}^{+}=R_{i,k}^{-}$ $(k=1,\ 2)$, the following steady-state equations can be derived according to (5):

$$\begin{cases} L_1\frac{di_{L1}}{dt}+i_{L1}\left(R_{i1}^{+}+R_{i1}^{-}\right)+i\left(R_{o1}^{+}+R_{o1}^{-}+2R\right)=2d_a v_{\mathrm{dc}} \\ L_2\frac{di_{L2}}{dt}+i_{L2}\left(R_{i2}^{+}+R_{i2}^{-}\right)+i\left(R_{o2}^{+}+R_{o2}^{-}+2R\right)=2d_b v_{\mathrm{dc}} \\ i_{L1}\left(R_{i1}^{+}+R_{i1}^{-}\right)+2iR_{o1}^{-}-i_{L2}\left(R_{i2}^{+}+R_{i2}^{-}\right) \\ \qquad -2iR_{o2}^{-}=2\left(d_a-d_b\right)v_{\mathrm{dc}} \\ v_{o1}=i\left(R_{o1}^{+}+R_{o1}^{-}+2R\right),\ v_{o2}=i\left(R_{o2}^{+}+R_{o2}^{-}+2R\right) \\ i_{L1}=i+C_1\frac{dv_{o1}}{dt},\quad i_{L2}=i+C_2\frac{dv_{o2}}{dt}. \end{cases} \tag{13}$$

Equation (13) cannot hold unless

$$L_1\frac{di_{L1}}{dt}-L_2\frac{di_{L2}}{dt}=i\left[\left(R_{o2}^{+}-R_{o2}^{-}\right)-\left(R_{o1}^{+}-R_{o1}^{-}\right)\right]. \tag{14}$$

Let $v_{o1}=V\sin(\omega t)$; according to (13), the following solutions can be obtained:

$$\begin{cases} i=\frac{V\sin(\omega t)}{\left(R_{o1}^{+}+R_{o1}^{-}+2R\right)} \\ v_{o2}=\frac{R_{o2}^{+}+R_{o2}^{-}+2R}{\left(R_{o1}^{+}+R_{o1}^{-}+2R\right)}V\sin(\omega t) \\ i_{L1}=\frac{V\sin(\omega t)}{\left(R_{o1}^{+}+R_{o1}^{-}+2R\right)}+\omega C_1 V\cos(\omega t) \\ i_{L2}=\frac{V\sin(\omega t)}{\left(R_{o1}^{+}+R_{o1}^{-}+2R\right)}+\frac{R_{o1}^{+}+R_{o1}^{-}+2R}{\left(R_{o1}^{+}+R_{o1}^{-}+2R\right)}\omega C_2 V\cos(\omega t) \end{cases}. \tag{15}$$

According to (15), if (14) holds, these conditions $L_1=L_2$ and $\omega^2 L_2\quad C_2(R_{o2}^{+}+R_{o2}^{-}+2R)-\omega^2 L_1\quad C_1(R_{o1}^{+}+R_{o1}^{-}+2R)=(R_{o2}^{+}-R_{o2}^{-})-(R_{o1}^{+}-R_{o1}^{-})$ must be met. Hence, for the gen-

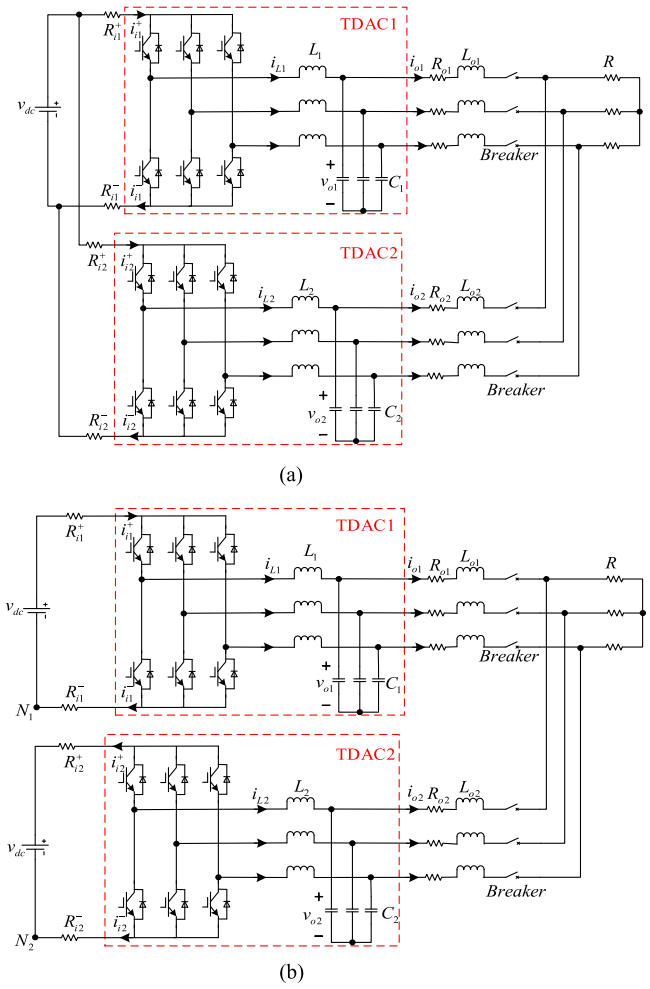

Fig. 12. Structures of two TDACs connected in (a) the IPOP form and (b) the ISOP form.

eral cases, all types of circulating currents among IPOP SDACs cannot be eliminated completely based on the bipolar modulation and only specific types of circulating currents can be eliminated.

IV. Circulating Currents Among IPOP Nonisolated TDACs

The TDACs are used to realize the mutual conversion between ac power and dc power for the medium-voltage industrial power. The topologies of TDACs are various, this section mainly focuses on typical nonisolated TDACs, which are widely used in practice with their mature control technologies. For convenience, we illustrate related problems through two IPOP TDACs, but the methods and conclusions can be extended to N ($N > 2$) IPOP TDACs with more complicated expressions.

The structure of two IPOP TDACs is shown in Fig. 12(a). The two SDACs operate in coordination to provide power for the load R. The outputs of TDACs are filtered by LC filters whose inductances are $L_1^{a,b,c}$ and $L_2^{a,b,c}$, capacitances are $C_1^{a,b,c}$ and $C_2^{a,b,c}$, respectively. The input voltage is $v_{\rm dc}$. The positive input line resistances are R_{i1}^{+} and R_{i2}^{+}, respectively, while the negative input line resistances are R_{i1}^{-} and R_{i2}^{-}, respectively.

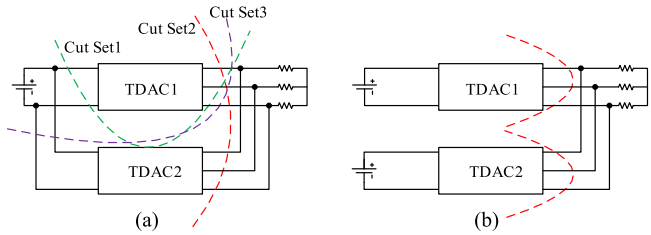

Fig. 13. Differences between IPOP TDACs and ISOP TDACs. (a) Currents coupling of IPOP TDACs. (b) Currents decoupling of ISOP TDACs.

The output line resistances are $R_{o1}^{a,b,c}$ and $R_{o2}^{a,b,c}$, respectively; the output line inductances are $L_{o1}^{a,b,c}$ and $L_{o2}^{a,b,c}$, respectively. The breakers of output terminals are used to protect the TDACs from faults. Fig. 12(b) shows the structure of two input-separated output-parallel (ISOP) TDACs, which are widely applied in microgrids to integrate different RESs into the power system. The meanings of corresponding notations are the same as those in Fig. 12(a). Comparing ISOP TDACs with IPOP TDACs, the essential difference is that the potentials of points N_1 and N_2 are clamped in IPOP TDACs, which will make the model of IPOP TDACs totally different from that of ISOP TDACs.

Being similar to the analysis of IPOP BDDCs and SDACs, the currents of IPOP TDACs are coupled together. As Fig. 13(a) shows, according to Kirchhoff's laws, the sum of output currents and input currents of cut set1 is zero, that is, $i_{o1}^{a} + i_{o1}^{b} + i_{o1}^{c} = i_{i1}^{+} - i_{i1}^{-}$, which means that $i_{o1}^{a} + i_{o1}^{b} + i_{o1}^{c} \neq 0$ could hold. In other words, for the IPOP TDACs, there will be zero-sequence circulating currents. Through the analyses of cut set2 and cut set3, similar conclusions can be obtained. This kind of explanation about the mechanism of zero-sequence circulating currents in three-phase system is very novel, which has never been mentioned in existing literatures. But for ISOP TDACs, there will be no zero-sequence circulating currents, which can be easily proven by the cut sets in Fig. 13(b). The zero-sequence circulating currents can be regarded as a big difference between IPOP TDACs and ISOP TDACs.

As analyzed in IPOP BDDCs and SDACs, not only the asymmetry of output terminal will cause the circulating currents, but also the asymmetry of input terminal could cause the circulating currents. The influences of output terminal are well researched by the existing literatures [24]–[27]; then this paper mainly focuses on the influences of input terminal, which are scarcely mentioned in existing literatures. The combinations of on–off states of TDAC1 and TDAC2 are very numerous, which reaches 64 operating stages. Hence, the complete mathematic model is very tedious to obtain. But the related problems can still be illustrated through some operating stages among total operating stages.

As shown in Fig. 14, which is one operating stage of two IPOP TDACs. For simplification, assuming that the parameters of these two TDACs in ac side are the same, but the input line resistances are asymmetric. If there are no circulating currents, then the potentials of a_1, b_1, c_1 and a_2, b_2, c_2 are different on account of the asymmetry of the input line resistances. These potential differences contradict with the assumption that there

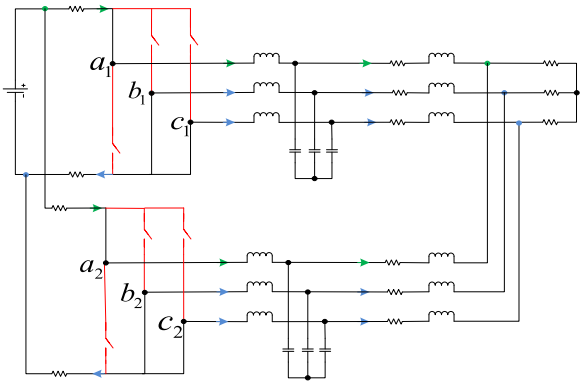

Fig. 14. One operating stage of two IPOP TDACs.

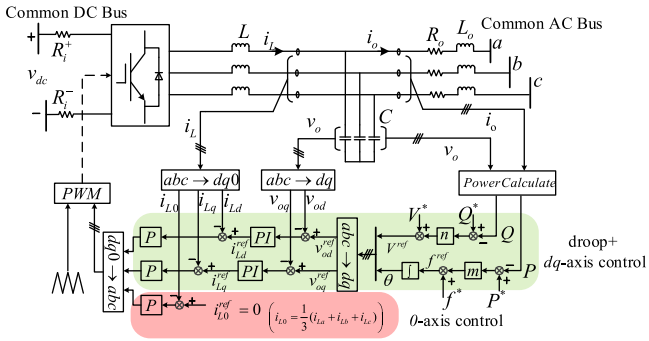

Fig. 15. Droop plus d–q–0 three-axis control.

are no circulating currents, because the output line impedances in the ac side are the same, the differences of potentials of a_1, b_1, c_1 and a_2, b_2, c_2 will cause circulating currents. Therefore, the assumption does not hold and there are circulating currents with the influences of input line resistances. On the other hand, the positive pole of input terminal of TDAC1 is connected in parallel with the positive pole of the input terminal of TDAC2, as shown by green arrows in Fig. 14, while the negative pole of input terminal of TDAC1 is connected in parallel with the negative pole of the input terminal of TDAC2, as shown by blue arrows in Fig. 14. Hence, the positive input currents and negative input currents may be not equal with asymmetric input line resistances. That is, zero-sequence circulating currents could occur because $i^a_{o,k} + i^b_{o,k} + i^c_{o,k} = i^+_{i,k} - i^-_{i,k}$ ($k = 1,\ 2$). In fact, the asymmetric input line resistances mainly cause zero-sequence circulating currents by the verification of experiments.

The circulating currents caused by the asymmetric input line resistances can be suppressed effectively by the droop plus d–q–0 three-axis control, as shown in Fig. 15, in which the 0-axis mainly control the zero-sequence components. Through introducing dc offsets in the modulation voltages, the IPOP TDACs will generate opposite circulating currents, and then the zero-sequence circulating currents can be suppressed effectively. With the droop control which can realize active and reactive power sharing, the currents among IPOP TDACs can be regulated well.

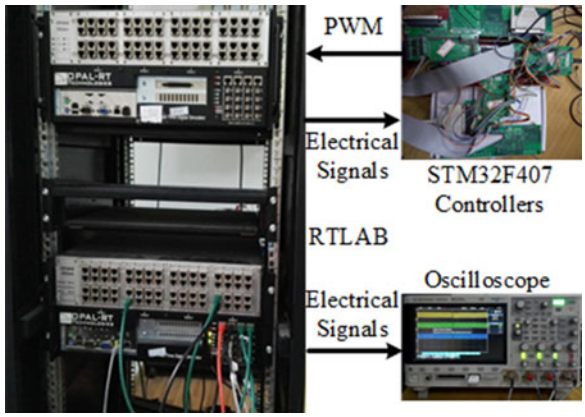

Fig. 16. HIL platform setup.

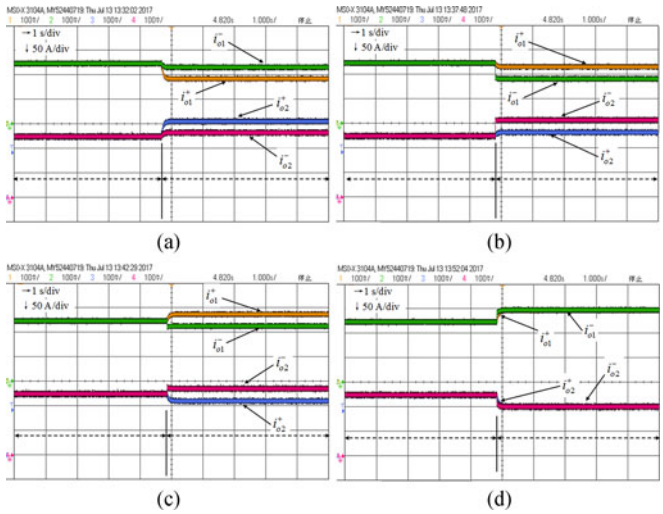

Fig. 17. Output currents of IPOP BDDCs with changes of output line resistances from rated state to (a) state1: $R^+_{o1} = 15$ mΩ, $R^-_{o1} = 10$ mΩ, $R^+_{o2} = 5$ mΩ, $R^-_{o2} = 10$ mΩ; (b) state2: $R^+_{o1} = 10$ mΩ, $R^-_{o1} = 15$ mΩ, $R^+_{o2} = 10$ mΩ, $R^-_{o2} = 5$ mΩ; (c) state3: $R^+_{o1} = 5$ mΩ, $R^-_{o1} = 15$ mΩ, $R^+_{o2} = 10$ mΩ, $R^-_{o2} = 10$ mΩ; (4) state4: $R^+_{o1} = 5$ mΩ, $R^-_{o1} = 5$ mΩ, $R^+_{o2} = 10$ mΩ, $R^-_{o2} = 10$ mΩ.

V. Hardware-in-Loop Tests

To verify the effectiveness of the earlier theoretical analyses, the corresponding HIL tests are conducted. The HIL platform is based on the RTLAB and STM32F407 MCUs. The equipment of the HIL platform is shown in Fig. 16.

A. IPOP BDDCs

The topology of the tested IPOP BDDCs is the same as Fig. 2(a), and the rated parameters are designed as the same as given in Table I.

Fig. 17 shows the output currents of IPOP BDDCs with the changes of output line resistances under the open-loop control, where the duty ratio is the same as given in Table I. In the rated state, $R^+_{o1} = R^-_{o1} = R^+_{o2} = R^-_{o2} = 10$ mΩ. In state1, $R^+_{o1} = 15$ mΩ, $R^-_{o1} = 10$ mΩ, $R^+_{o2} = 5$ mΩ, and $R^-_{o2} = 10$ mΩ to test the influence of asymmetry of positive output line resistances. In state2, $R^+_{o1} = 10$ mΩ, $R^-_{o1} = 15$ mΩ, $R^+_{o2} = 10$ mΩ, and $R^-_{o2} = 5$ mΩ to test the influence of

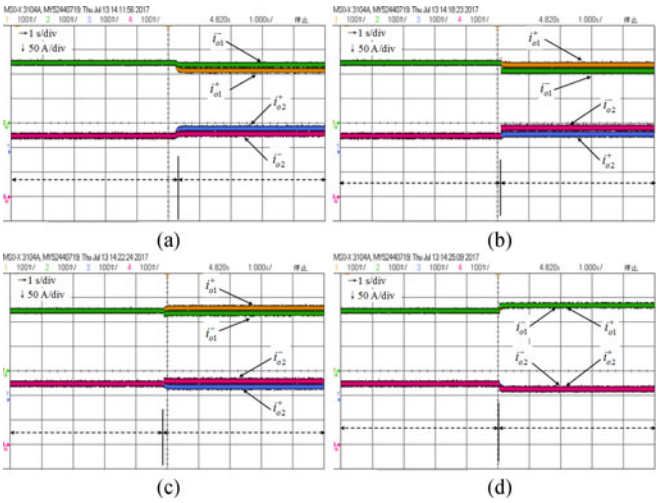

Fig. 18. Output currents of IPOP BDDCs with changes of input line resistances from rated state to (a) state1: $R_{i1}^{+} = 15\ \text{m}\Omega$, $R_{i1}^{-} = 10\ \text{m}\Omega$, $R_{i2}^{+} = 5\ \text{m}\Omega$, $R_{i2}^{-} = 10\ \text{m}\Omega$; (b) state2: $R_{i1}^{+} = 10\ \text{m}\Omega$, $R_{i1}^{-} = 15\ \text{m}\Omega$, $R_{i2}^{+} = 10\ \text{m}\Omega$, $R_{i2}^{-} = 5\ \text{m}\Omega$; (c) state3: $R_{i1}^{+} = 5\ \text{m}\Omega$, $R_{i1}^{-} = 15\ \text{m}\Omega$, $R_{i2}^{+} = 10\ \text{m}\Omega$, $R_{i2}^{-} = 10\ \text{m}\Omega$; (4) state4: $R_{i1}^{+} = 5\ \text{m}\Omega$, $R_{i1}^{-} = 5\ \text{m}\Omega$, $R_{i2}^{+} = 10\ \text{m}\Omega$, $R_{i2}^{-} = 10\ \text{m}\Omega$.

asymmetry of negative output line resistances. In state3, $R_{o1}^{+} = 5\ \text{m}\Omega$, $R_{o1}^{-} = 15\ \text{m}\Omega$, $R_{o2}^{+} = 10\ \text{m}\Omega$, and $R_{o2}^{-} = 10\ \text{m}\Omega$ to test the influence of asymmetry of positive and negative output line resistances in individual BDDC. In state4, $R_{o1}^{+} = R_{o1}^{-} = 5\ \text{m}\Omega$, $R_{o2}^{+} = R_{o2}^{-} = 10\ \text{m}\Omega$ to test the influence of asymmetry of output line resistances of two BDDCs. Fig. 18 shows the output currents of IPOP BDDCs with the changes of input line resistances under the open-loop control, where the constant duty ratio is the same as given in Table I. The designed test states are similar to Fig. 17. Only the output line resistances are replaced with the input line resistances.

From the results, it can be concluded that the asymmetry of line resistance will cause serious circulating currents among IPOP BDDCs, which include multiple types like $i_{o1}^{+} - i_{o2}^{+}$ (two positive poles), $i_{o1}^{-} - i_{o2}^{-}$ (two negative poles), $i_{o1}^{+} - i_{o1}^{-}$, and $i_{o2}^{+} - i_{o2}^{-}$ (inner circulating currents). Compared to the output currents of ISOP BDDCs, the output currents of IPOP BDDCs are much more complex. Especially, the port degradation is very obvious, that is, $i_{o1}^{+} \neq i_{o1}^{-}$ or $i_{o2}^{+} \neq i_{o2}^{-}$ when there is asymmetry of the positive and negative line resistances in individual BDDC. On the other hand, comparing Figs. 17 with 18, it can be seen that the influences of input line resistances are less than the influences of output line resistances.

The different kinds of asymmetry of line resistances have different sensitivity on various circulating currents. As Figs. 17(a) and 18(a) show, the asymmetry of positive line resistances influences the circulating currents between two positive poles greatly, while as Figs. 17(b) and 18(b) show, the asymmetry of negative line resistances influences the circulating currents between two negative poles greatly. For the inner circulating currents, if both the positive and negative line resistances of individual BDDC can be kept the same, this kind of circulating currents can be eliminated, as Figs. 17(d) and 18(d) show.

Furthermore, unlike the ISOP BDDCs, even though $R_{o1}^{+} + R_{o1}^{-} = R_{o2}^{+} + R_{o2}^{-}$ and $R_{i1}^{+} + R_{i1}^{-} = R_{i2}^{+} + R_{i2}^{-}$, the circulating currents still exist, as Figs. 17(c) and 18(c) show. Hence, the suppression of circulating currents among IPOP BDDCs is harder than that of ISOP BDDCs.

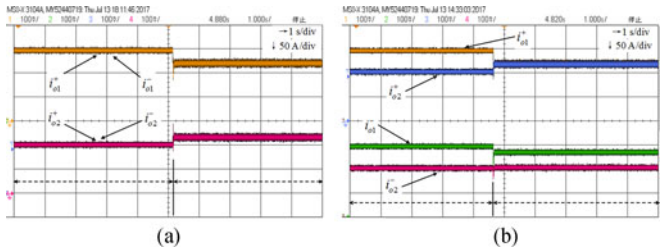

Fig. 19. Output currents of BDDCs before and after droop control is enabled. (a) ISOP BDDCs. (b) IPOP BDDCs.

Fig. 19 shows the control effects of droop control when it is applied into ISOP BDDCs and IPOP BDDCs. The topology of the tested ISOP BDDCs is presented in Fig. 2(b). The parameters of two kinds of BDDCs are the same. $R_{o1}^{+} = R_{o1}^{-} = 5\ \text{m}\Omega$, $R_{o2}^{+} = R_{o2}^{-} = 10\ \text{m}\Omega$, and the other parameters are the same as Table I. The droop coefficients of two BDDCs are set as $0.2\ \text{V/A}$, which is much larger than the line resistance. Fig. 19(a) shows the control effects of droop control in ISOP BDDCs. As the figure shows, before the droop control is enabled, $i_{o1}^{+} = i_{o1}^{-} = 150\ \text{A}$, $i_{o2}^{+} = i_{o2}^{-} = 100\ \text{A}$. After the droop control is enabled, $i_{o1}^{+} = i_{o1}^{-} = 125\ \text{A}$, $i_{o2}^{+} = i_{o2}^{-} = 125\ \text{A}$. That is, the output currents of ISOP BDDCs become equal and circulating currents are suppressed effectively. Fig. 19(b) shows the control effects of droop control in IPOP BDDCs. As the figure shows, before the droop control is enabled, $i_{o1}^{+} = i_{o1}^{-} = 150\ \text{A}$, $i_{o2}^{+} = i_{o2}^{-} = 100\ \text{A}$. After the droop control is enabled, $i_{o1}^{+} = i_{o2}^{+} = 125\ \text{A}$, $i_{o1}^{-} = 140\ \text{A}$, and $i_{o2}^{-} = 110\ \text{A}$. The two positive output currents of IPOP BDDCs became equal, but the negative output currents are still unequal. Therefore, the conventional droop control cannot completely suppress the circulating currents among IPOP BDDCs.

B. IPOP SDACs

The topology of the tested IPOP SDACs is the same as Fig. 7(a), and the rated parameters are designed as the same as Table II.

Fig. 20 shows the output currents of IPOP SDACs with the changes of output line resistances under the open-loop control, where the modulation mode is bipolar and the duty ratio is the same as Table II. In the rated state, $R_{o1}^{+} = R_{o1}^{-} = R_{o2}^{+} = R_{o2}^{-} = 10\ \text{m}\Omega$. In state1, $R_{o1}^{+} = 18\ \text{m}\Omega$, $R_{o1}^{-} = 10\ \text{m}\Omega$, $R_{o2}^{+} = 2\ \text{m}\Omega$, $R_{o2}^{-} = 10\ \text{m}\Omega$ to test the influence of asymmetry of positive output line resistances. In state2, $R_{o1}^{+} = 10\ \text{m}\Omega$, $R_{o1}^{-} = 18\ \text{m}\Omega$, $R_{o2}^{+} = 10\ \text{m}\Omega$, $R_{o2}^{-} = 2\ \text{m}\Omega$ to test the influence of asymmetry of negative output line resistances. In state3, $R_{o1}^{+} = 2\ \text{m}\Omega$, $R_{o1}^{-} = 18\ \text{m}\Omega$, $R_{o2}^{+} = 10\ \text{m}\Omega$, $R_{o2}^{-} = 10\ \text{m}\Omega$ to test the influence of asymmetry of positive and negative output line resistances in individual SDAC. In state4, $R_{o1}^{+} = R_{o1}^{-} = 2\ \text{m}\Omega$, $R_{o2}^{+} = R_{o2}^{-} = 10\ \text{m}\Omega$ to test the influence of asymmetry of output line resistances of two SDACs.

From the results, it can be concluded that the asymmetry of output line resistance will cause various kinds of circulating

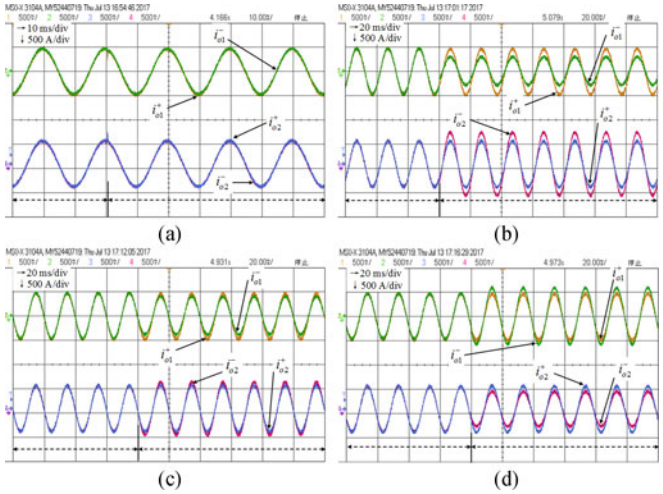

Fig. 20. Output currents of IPOP SDACs with changes of output line resistances from rated state to (a) state1: $R_{o1}^{+} = 18$ mΩ, $R_{o1}^{-} = 10$ mΩ, $R_{o2}^{+} = 2$ mΩ, $R_{o2}^{-} = 10$ mΩ; (b) state2: $R_{o1}^{+} = 10$ mΩ, $R_{o1}^{-} = 18$ mΩ, $R_{o2}^{+} = 10$ mΩ, $R_{o2}^{-} = 2$ mΩ; (c) state3: $R_{o1}^{+} = 2$ mΩ, $R_{o1}^{-} = 18$ mΩ, $R_{o2}^{+} = 10$ mΩ, $R_{o2}^{-} = 10$ mΩ; (4) state4: $R_{o1}^{+} = 2$ mΩ, $R_{o1}^{-} = 2$ mΩ, $R_{o2}^{+} = 10$ mΩ, $R_{o2}^{-} = 10$ mΩ.

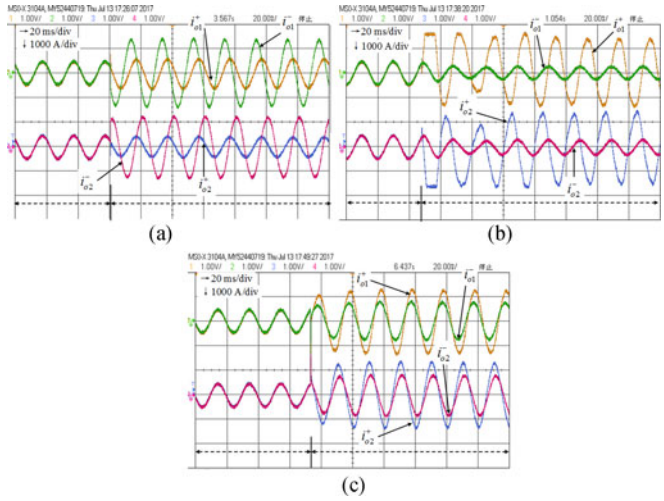

Fig. 21. Output currents of IPOP SDACs with changes of input line resistances and filters. (a) From the rated sate to $R_{i1}^{+} = R_{i1}^{-} = 2$ mΩ, $R_{i2}^{+} = R_{i2}^{-} = 10$ mΩ. (b) From the rated sate to $L_1 = 1.5$ mH and $L_2 = 0.5$ mH. (c) From the rated sate to $C_1 = 10$ mF and $C_2 = 6$ mF.

currents among IPOP SDACs with different sensitivity. Compared to the output currents of IPOS SDACs, the output currents of IPOP SDACs are relatively complex. Especially, the port degradation is obvious and becomes complicated. Unlike the IPOP BDDCs, even though the positive and negative output line resistances of individual SDAC are kept the same, the port degradation is still existing, that is, $i_{o1}^{+} \neq i_{o1}^{-}$ or $i_{o2}^{+} \neq i_{o2}^{-}$, as Fig. 20(d) shows.

As Fig. 20(a) shows, the asymmetry of positive output line resistances has less influences on the output currents. But the asymmetry of negative output line resistances has great influences on the output currents, as shown in Fig. 20(b). Furthermore, unlike the IPOS SDACs, even though $R_{o1}^{+} + R_{o1}^{-} = R_{o2}^{+} + R_{o2}^{-}$ and $R_{i1}^{+} + R_{i1}^{-} = R_{i2}^{+} + R_{i2}^{-}$, the circulating currents still exist, as Fig. 20(c) shows. Hence, the suppression of circulating currents among IPOP SDACs is harder than that of IPOS SDACs.

As analyzed in Section III, the positive and negative input line resistances of individual SDAC must be the same else the IPOP SDACs are unstable. Hence, for the input line resistances, only the test state where $R_{i1}^{+} = R_{i1}^{-} = 2$ mΩ, $R_{i2}^{+} = R_{i2}^{-} = 10$ mΩ is conducted to test the influence of asymmetry of input line resistances. Fig. 21(a) shows the output currents from rated state to this test state. From the result, it can be concluded that the input line resistances have great influences on circulating currents compared to the output line resistances. The influences of filters are shown in Fig. 21(b) and (c), where $L_1 = 1.5$ mH and $L_2 = 0.5$ mH, $C_1 = 10$ mF and $C_2 = 6$ mF, respectively.

Fig. 22 shows the influence of asymmetry of positive and negative input line resistances in individual SDAC, where the test state is that $R_{i1}^{+} = 2$ mΩ, $R_{i1}^{-} = 18$ mΩ, $R_{i2}^{+} = 10$ mΩ, and $R_{i2}^{-} = 10$ mΩ. Fig. 22(a) shows that the asymmetry of positive and negative input line resistances will make IPOP SDACs unstable. But for IPOS SDACs whose topology is shown in Fig. 7(b), the asymmetry of positive and negative input line

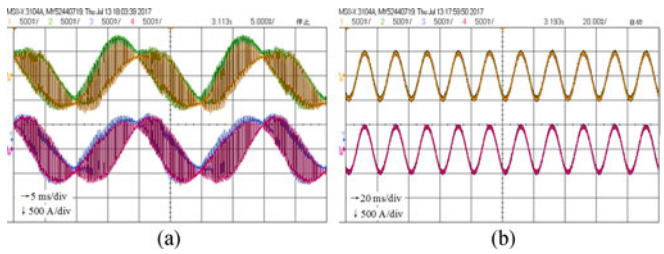

Fig. 22. Influence of asymmetry of positive and negative input line resistances in individual SDAC ($R_{i1}^{+} = 2$ mΩ, $R_{i1}^{-} = 18$ mΩ, $R_{i2}^{+} = 10$ mΩ, $R_{i2}^{-} = 10$ mΩ). (a) IPOP SDACs. (b) IPOS SDACs.

resistances does not cause instability, as Fig. 22(b) shows. This phenomenon means that the IPOP SADCs are essentially different from the IPOS or ISOP SDACs.

C. IPOP TDACs

The topology of the tested IPOP TDACs is the same as shown in Fig. 12(a), and the control block diagram is the same as shown in Fig. 15. The parameters are as follows. DC voltage $v_{\mathrm{dc}} = 1000$ V; rated ac voltage and frequency are 311 V and 50 Hz, respectively; ac load is 20 kW; input line resistances are asymmetric, $R_{i1}^{+} = 5$ mΩ, $R_{i1}^{-} = 15$ mΩ, $R_{i2}^{+} = R_{i2}^{-} = 10$ mΩ; output line impedances are symmetric, $R_{o1} = R_{o2} = 1$ mΩ, $L_{o1} = L_{o2} = 1$ mH; LC filters of two TDACs are designed the same, $L_1 = L_2 = 1$ mH, $C_1 = C_2 = 5$ mF; droop controller: $P_1^{*} = P_2^{*} = 5$ kW, $Q_1^{*} = Q_2^{*} = 0$ kW, $m_1 = m_2 = 0.025$ Hz/kW, $n_1 = n_2 = 0.1$ V/kVar; inner loops of two TDACs are designed the same; voltage controller: $k_{PV} = 0.8$ A/V, $k_{IV} = 800$ A/Vs; and current controller: $k_{PC} = 0.01$ V/A.

Fig. 23 shows the output currents of IPOP TDACs. Fig. 23(a) shows the three-phase output currents of TDAC1. When only the d–q axis-based droop control is applied, it can be seen that there are great zero-sequence components because of the asymmetry of input line resistances. But when the d–q–0 axis-based

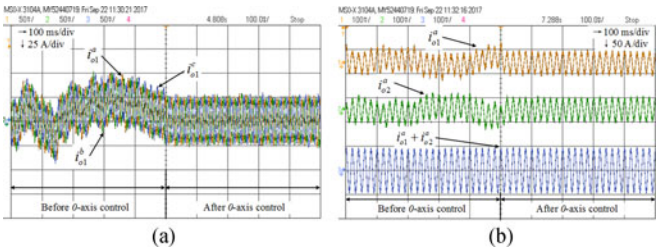

(a) (b)

Fig. 23. Control effects of *d*–*q*–0 axis-based droop control when the input line resistances are asymmetric in IPOP TDACs: (a) three-phase output currents of TDAC1 and (b) *a*-phase currents of two TDACs.

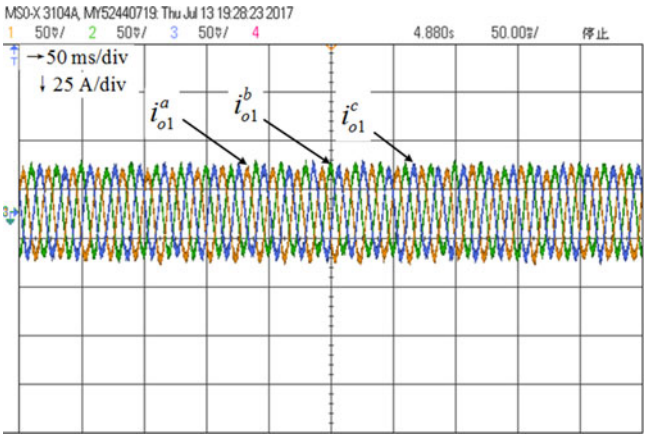

Fig. 24. Three-phase output currents of TDAC1 of ISOP TDACs with only the *d*–*q* axis-based droop control.

droop control is applied, it can be seen that the zero-sequence components are suppressed effectively. Fig. 23(b) shows the *a*-phase output currents of TDAC1, TDAC2, and the sum of them. If only the *d*–*q* axis-based droop control is applied, the output currents of two TDACs are fluctuating with great dc offsets, but the sum of them is normal. It means that there are circulating currents between these two TDACs. After the *d*–*q*–0 axis-based droop control is applied, the output currents of two TDACs become normal and equal, and at the same time, the dc offsets are greatly decreased.

Fig. 24 shows that the asymmetry of input line resistances will not result in circulating currents among ISOP TDACs, whose topology is shown in Fig. 12(b). The test parameters are the same as shown in Fig. 23, and only the *d*–*q* axis-based droop control is applied. This phenomenon means that the IPOP TDACs and ISOP TDACs have great differences.

VI. Conclusion

The circulating currents of IPOP nonisolated BDDCs, SDACs, and TDACs are modeled and analyzed in this paper, which are the main challenge when these nonisolated converters are applied into hybrid ac/dc distribution network. First, the detailed mathematic models of circulating currents are derived through a unified modeling approach. Through comparison, it can be found that the models of IPOP converters are very complicated and are greatly different from the models of ISOP or IPOS converters. The complicated characteristics and the generation mechanism of circulating currents are clearly explained. Second, based on the models, it can be concluded that circulating currents will cause port degradation, which will make some port-based control methods ineffective and influence the relay protection. Also, the corresponding influence factors like line resistances, filters, and so on, are analyzed in detail. Through numerical analysis, the asymmetry of line resistances has great influences on circulating currents and results in more complex circulating currents than that in ISOP or IPOS converters. Then, some traditional control methods cannot eliminate these circulating currents completely. Especially for the IPOP SDACs, the asymmetry of input line resistances will cause instability. At last, the real-time HIL tests are conducted to verify the effectiveness of the theoretical analyses. We hope that these essential works can make contributions to more effective suppression strategies of circulating currents among IPOP nonisolated converters.

References

[1] F. Nejabatkhah and Y. W. Li, "Overview of power management strategies of hybrid AC/DC microgrid," *IEEE Trans. Power Electron.*, vol. 30, no. 12, pp. 7072–7089, Dec. 2015.

[2] X. Liu, P. Wang, and P. C. Loh, "A hybrid AC/DC microgrid and its coordination control," *IEEE Trans. Smart Grid*, vol. 2, no. 2, pp. 278–286, Jun. 2011.

[3] P. C. Loh, D. Li, Y. K. Chai, and F. Blaabjerg, "Autonomous Operation of Hybrid Microgrid With AC and DC Subgrids," *IEEE Trans. Power Electron.*, vol. 28, no. 5, pp. 2214–2223, May 2013.

[4] Y. Xia, Y. Peng, P. Yang, M. Yu, and W. Wei, "Distributed coordination control for multiple bidirectional power converters in a hybrid AC/DC microgrid," *IEEE Trans. Power Electron.*, vol. 32, no. 6, pp. 4949–4959, Jun. 2017.

[5] L. Asiminoaei, E. Aeloiza, P. N. Enjeti, and F. Blaabjerg, "Shunt active-power-filter topology based on parallel interleaved inverters," *IEEE Trans. Ind. Electron.*, vol. 55, no. 3, pp. 1175–1189, Mar. 2008.

[6] Y. Xia, W. Wei, Y. Peng, P. Yang, and M. Yu, "Decentralized coordination control for parallel bidirectional power converters in a grid-connected DC microgrid," *IEEE Trans. Smart Grid*, doi: 10.1109/TSG.2017.2725987.

[7] J. Shi, L. Zhou, and X. He, "Common-duty-ratio control of input-parallel output-parallel (IPOP) connected DC–DC converter modules with automatic sharing of currents," *IEEE Trans. Power Electron.*, vol. 27, no. 7, pp. 3277–3291, Jul. 2012.

[8] J. Shi, T. Liu, J. Cheng, and X. He, "Automatic current sharing of an input-parallel output-parallel (IPOP)-connected DC–DC converter system with chain-connected rectifiers," *IEEE Trans. Power Electron.*, vol. 30, no. 6, pp. 2997–3016, Jun. 2015.

[9] B. R. Lin and C. W. Chu, "DC/DC converter with parallel input and parallel output with shared power switches and rectifier diodes," *IET Power Electron.*, vol. 8, no. 5, pp. 814–821, May 2015.

[10] D. Liu, F. Deng, Z. Gong, and Z. Chen, "Input-parallel output-parallel (IPOP) three-level (TL) DC/DC converters with interleaving control strategy for minimizing and balancing capacitor ripple currents," *IEEE J. Emerg. Sel. Topics Power Electron.*, doi: 10.1109/JESTPE.2017.2649221.

[11] C. Liu *et al.*, "Magnetic-coupling current-balancing cells based input-parallel output-parallel LLC resonant converter modules for high-frequency isolation of DC distribution systems," *IEEE Trans. Power Electron.*, vol. 31, no. 10, pp. 6968–6979, Oct. 2016.

[12] J. Gordillo and C. Aguilar, "A simple sensorless current sharing technique for multiphase DC–DC buck converters," *IEEE Trans. Power Electron.*, vol. 32, no. 5, pp. 3480–3489, May 2017.

[13] H. Mao, L. Yao, C. Wang, and I. Batarseh, "Analysis of inductor current sharing in nonisolated and isolated multiphase dc–dc converters," *IEEE Trans. Ind. Electron.*, vol. 54, no. 6, pp. 3379–3388, Dec. 2007.

[14] A. C. Schittler, D. Pappis, C. Rech, A. Campos, and M. A. Dalla Costa, "Generalized state-space model for the interleaved buck converter," in *Proc. XI Brazilian Power Electron. Conf.*, 2011, pp. 451–457.

[15] Y. H. Liao, H. C. Chen, and H. C. Cheng, "Common mode and differential mode circulating-current control in paralleled single-phase boost rectifiers," in *Proc. IEEE APEC*, 2013, pp. 361–367.

[16] Z. Ye, P. K. Jain, and P. C. Sen, "Circulating current minimization in high-frequency AC power distribution architecture with multiple inverter modules operated in parallel," *IEEE Trans. Ind. Electron.*, vol. 54, no. 5, pp. 2673–2687, Oct. 2007.
[17] Y. H. Liao, H. C. Chen, H. C. Cheng, and C. M. Lai, "A novel control strategy of circulating currents in parallel single-phase boost rectifiers," in *Proc. IEEE APEC*, 2012, pp. 1034–1041.
[18] Y. H. Liao, H. C. Chen, H. C. Cheng, Y. L. Ke, and Y. T. Li, "A novel control strategy of circulating currents in paralleled single-phase boost converters with different power sharing for microgrid applications," *IEEE Trans. Ind. Appl.*, vol. 50, no. 2, pp. 1304–1312, Mar. 2014.
[19] Y. H. Liao and H. C. Chen, "Simplified PWM with switching constraint method to prevent circulating currents for paralleled bidirectional AC/DC converters in grid-tied system using graphic analysis," *IEEE Trans. Ind. Electron.*, vol. 62, no. 7, pp. 4573–4586, Jul. 2015.
[20] Z. Ye, D. Boroyevich, J. Y. Choi, and F. C. Lee, "Control of circulating current in two parallel three-phase boost rectifiers," *IEEE Trans. Power Electron.*, vol. 17, no. 5, pp. 609–615, Sep. 2002.
[21] X. Zhang, J. Chen, Y. Ma, Y. Wang, and D. Xu, "Bandwidth expansion method for circulating current control in parallel three-phase PWM converter connection system," *IEEE Trans. Power Electron.*, vol. 29, no. 12, pp. 6847–6856, Dec. 2014.
[22] R. Zhu, M. Liserre, Z. Chen, and X. Wu, "Zero-sequence voltage modulation strategy for multiparallel converters circulating current suppression," *IEEE Trans. Ind. Electron.*, vol. 64, no. 3, pp. 1841–1852, Mar. 2017.
[23] B. Wei, J. M. Guerrero, J. C. Vásquez, and X. Guo, "A circulating-current suppression method for parallel-connected voltage-source inverters with common DC and AC Buses," *IEEE Trans. Ind. Appl.*, vol. 53, no. 4, pp. 3758–3769, Aug. 2017.
[24] C. T. Pan and Y. H. Liao, "Modeling and coordinate control of circulating currents in parallel three-phase boost rectifiers," *IEEE Trans. Ind. Electron.*, vol. 54, no. 2, pp. 825–838, Apr. 2007.
[25] X. Zhang, T. Wang, X. Wang, G. Wang, Z. Chen, and D. Xu, "A coordinate control strategy for circulating current suppression in multiparalleled three-phase inverters," *IEEE Trans. Ind. Electron.*, vol. 64, no. 1, pp. 838–847, Jan. 2017.
[26] Z. Quan and Y. Li, "Suppressing zero-sequence circulating current of modular interleaved three-phase converters using carrier phase shift PWM," *IEEE Trans. Ind. Appl.*, vol. 53, no. 4, pp. 3782–3792, Jul.–Aug. 2017, doi: 10.1109/TIA.2017.2683446.
[27] F. Wang, Y. Wang, Q. Gao, C. Wang, and Y. Liu, "A Control strategy for suppressing circulating currents in parallel-connected PMSM drives with individual DC links," *IEEE Trans. Power Electron.*, vol. 31, no. 2, pp. 1680–1691, Feb. 2016.
[28] X. Wang, Y. Peng, J. Zhu, Y. Xia, M. Yu, H. Hu, H. Cai, and W. Wei, "Decentralized impedance specifications for small-signal stability of DC distributed power systems," *IEEE J. Emerg. Sel. Topics Power Electron.*, vol. 5, no. 4, pp. 1578–1588, Dec. 2017.
[29] X. Zhang, X. Ruan, and C. K. Tse, "Impedance-based local stability criterion for DC distributed power systems, " *IEEE Trans. Circuits Syst. I, Reg. Papers*, vol. 62, no. 3, pp. 916–925, Jan. 2015.
[30] F. Ji, J. Xiang, W. Li, and Q. Yue, "A feedback passivation design for DC microgrid and its DC/DC converters," *Energies*, vol. 10, no. 1, pp. 14–29, Dec. 2016.
[31] Y. Gu, W. Li, and X. He, "Passivity-based control of DC microgrid for self-disciplined stabilization," *IEEE Trans. Power Electron.*, vol. 30, no. 5, pp. 2623–2632, Sep. 2015.

Yanghong Xia (S'16) was born in Hubei Province, China, in 1991. He received the B.S. degree in automation from the College of Automation, Huazhong University of Science and Technology, Wuhan, China, in 2014. He is currently working toward the Ph.D. degree in the College of Electrical Engineering, Zhejiang University, Hangzhou, China.

His current research interests include nonlinear control, distributed generations, and microgrids.

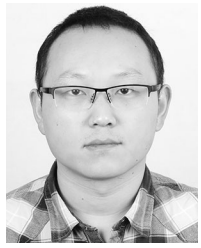

Miao Yu (M'16) received the B.S. degree in automation and the Ph.D. degree in control science and engineering from the College of Electrical Engineering, Zhejiang University, Hangzhou, China, in 2007 and 2012, respectively.

From 2013 to 2015, he was a Postdoctoral Researcher with Aalto University, Espoo, Finland. Since 2016, he has been a Lecturer with the College of Electrical Engineering, Zhejiang University. He has authored or coauthored more than 30 technical papers in journals and conferences. His current research interests include control strategies in microgrids and renewable power generation.

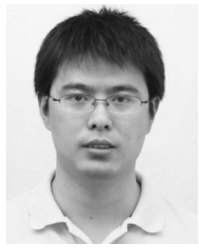

Yonggang Peng (M'16) received the B.Eng., M.Eng., and D.Eng. degrees in control theory and control engineering all from the College of Electrical Engineering, Zhejiang University, Hangzhou, China, in 2001, 2004, and 2008, respectively.

He is currently a Professor with the College of Electrical Engineering, Zhejiang University. His current research interests include distributed generations, microgrids, and intelligent control.

Wei Wei received the B.Eng., degree in automation, M.Eng., degree in control theory and control engineering and D.Eng. degree in power electronics and electronic drives all from the College of Electrical Engineering, Zhejiang University, Hangzhou, China, in 1983, 1986, and 1994, respectively.

Since 1986, he has been with the College of Electrical Engineering, Zhejiang University, where he is currently a Professor. His current research interests include intelligent control and the development of novel technology for renewable energy and smart grids.